



Is the Bounty Trough off eastern New Zealand an aborted rift?

J. W. G. Grobys,^{1,2} K. Gohl,¹ B. Davy,³ G. Uenzelmann-Neben,¹ T. Deen,^{4,5}
and D. Barker³

Received 19 December 2005; revised 21 August 2006; accepted 7 September 2006; published 22 March 2007.

[1] Remarkably little is known about the Cretaceous rifting process between New Zealand and Antarctica that affected the submarine regions within the New Zealand microcontinent. Bounty Trough provides insights into these breakup processes. Here we present results from a combined gravity, multichannel seismic, and wide-angle reflection/refraction seismic transect across the Middle Bounty Trough and interpret these results on the basis of velocity distribution and crustal composition derived from Poisson's ratio and P-wave velocity. The lower crust exhibits a high-velocity ($v_p \cong 7 - 7.7$ km/s, $v_s \cong 3.9 - 4.5$ km/s), high-density ($\rho = 3.02$ kg/cm³) body at the location of the thinnest crust on the profile. Here the crustal thickness is reduced to about 9 km from 22–24 km beneath Chatham Rise and Campbell Plateau. We interpret the high-velocity/density body as a magmatic intrusion into thinned continental crust. Our results show that the Cretaceous opening of Bounty Trough was very likely not the result of back-arc extension caused by collision of the Hikurangi Plateau with the Gondwana margin, but of continental breakup processes related to the separation of New Zealand from Antarctica. Rifting ceased in the Middle Bounty Trough at the onset of seafloor spreading. Comparisons with the Oslo Rift and the Ethiopian/Kenya Rift indicate that all three rift systems show analogous extensional features. From this we derive a stretching model for the Bounty Trough that combines elements of pure shear and simple shear extension.

Citation: Grobys, J. W. G., K. Gohl, B. Davy, G. Uenzelmann-Neben, T. Deen, and D. Barker (2007), Is the Bounty Trough off eastern New Zealand an aborted rift?, *J. Geophys. Res.*, 112, B03103, doi:10.1029/2005JB004229.

1. Introduction

[2] Rift systems play a key role in the Wilson Cycle and give important insights into the processes and driving mechanisms that control the breakup of continents [Woodcock, 2004]. Many conjugate margins exhibit a distinct asymmetry that is often correlated with detachment faults accommodating large strains during extension [Whitmarsh *et al.*, 2001]. Observations at rifts indicate that extension generally does not follow either of the accepted end-member extension models of “uniform stretching” or “simple shear” [Lister *et al.*, 1986], but may consist of a succession invoking both [Ro and Faleide, 1992]. Quantifying the amount of crustal stretching allows refinement of plate tectonic reconstructions, since most plate kinematic recon-

structions do not take into account rifting prior to seafloor spreading.

[3] The Bounty Trough is a bathymetric feature, up to 3 km deep, overlying a Cretaceous sedimentary basin in a submarine continental plateau. It separates the Campbell Plateau and Bounty Platform from the Chatham Rise (Figure 1). Thick (2 km) stratified sedimentary layers, which have mainly accumulated since the late Pliocene, characterize the modern Bounty Trough [Davey, 1977; Carter and Carter, 1987, 1993]. From seismic information, Carter *et al.* [1994] came to the conclusion that the Bounty Trough has a rift origin. Carter and Carter [1987] mentioned that new seafloor was not created within the rift, whereas Davy [1993] interpreted quasi-symmetric magnetic anomalies and rotated basement blocks as evidence for Permian back-arc/oceanic crust reworked by Cretaceous extension.

[4] A number of plate tectonic reconstructions of the region have been made on the basis of geological observations [Kamp, 1986], palinspastic reconstructions [Gray and Norton, 1988] and magnetic data [Sutherland, 1999; Eagles *et al.*, 2004]. While a Santonian to Campanian timing of Bounty Trough opening can be indirectly derived from geological and plate tectonic evidence [Wood and Herzer, 1993; Eagles *et al.*, 2004], the trough's role in the regional plate tectonic context is still poorly constrained.

¹Alfred Wegener Institute for Polar and Marine Research, Bremerhaven, Germany.

²Now at Federal Armed Forces Underwater Acoustics and Marine Geophysics Research Institute, Kiel, Germany.

³GNS Science, Lower Hutt, New Zealand.

⁴ARC National Key Research Centre for Geochemical Evolution and Metallogeny of Continents, Department of Earth and Planetary Sciences, Macquarie University, NSW, Australia.

⁵Now at British Antarctic Survey, Cambridge, UK.

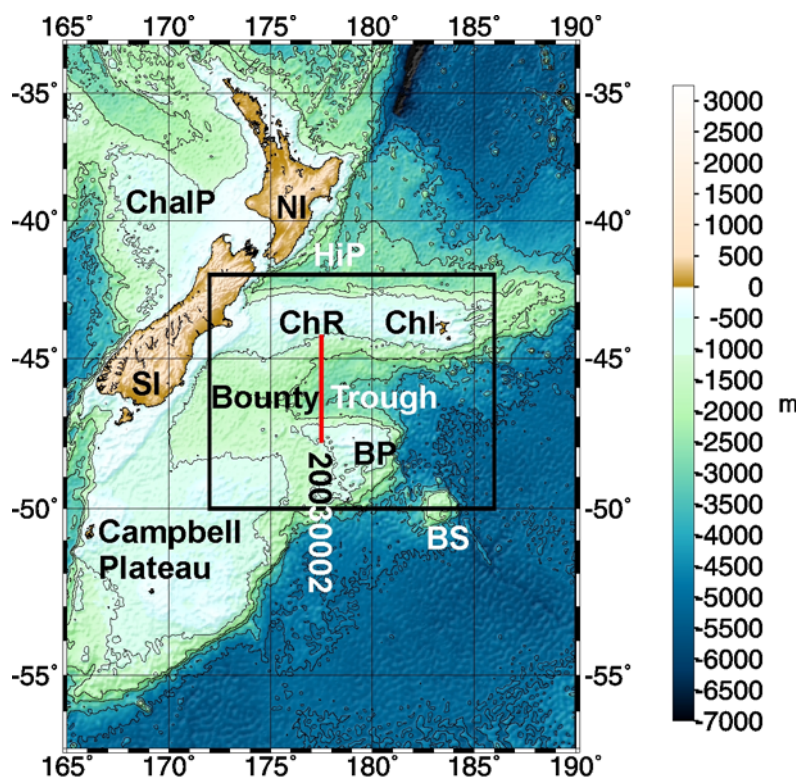


Figure 1. Bathymetric overview map [Smith and Sandwell, 1997] of the area southeast of the South Island of New Zealand and location of the CAMP experiment, showing location of seismic transect AWI-20030002 across the Bounty Trough (red). The black box shows the area of the gravimetric map (Figure 3). Abbreviations are NI: North Island of New Zealand, SI: South Island of New Zealand, ChR: Chatham Rise, BP: Bounty Platform, BS: Bollons Seamount, ChI: Chatham Islands, HiP: Hikurangi Plateau, and ChalP: Challenger Plateau.

[5] Knowledge of the regional rifting mechanisms may also improve the understanding of the differences between Marie Byrd Land and the New Zealand continent. Campbell Plateau and Chatham Rise rifted from the Marie Byrd Land and Ellsworth Land sectors of Antarctica. All of these regions, appear to have a similar crustal composition [Wandres *et al.*, 2004, and references therein], and crustal thickness (~ 25 km), but a different elevation relative to the sea surface [Ritzwoller *et al.*, 2001]. While Chatham Rise and the Campbell Plateau are submarine plateaus at 500 m depth or deeper, Marie Byrd Land rises at least 500 m above sea level [Winberry and Anandkrishnan, 2004], while a uniform elevation of the four crustal blocks mentioned above prior to rifting [LeMasurier and Landis, 1996] is suggested. An improved knowledge of the crustal structure and rifting process should contribute to our understanding of the differential uplift and/or subsidence processes. Knowledge of the composition and the opening/extensional history of the Bounty Trough is important because of the trough's key position in the reconstruction of the Gondwana breakup between Antarctica and New Zealand [Eagles *et al.*, 2004] (Figure 2). Whether the Bounty Trough is underlain by oceanic crust or thinned continental crust, and whether the Bounty Trough is a back-arc basin or a failed rift arm of a triple junction at its mouth are questions that are still under debate [Davy, 1993; Sutherland, 1999]. A better knowledge of the roles played by these different

processes will significantly improve plate kinematic models of the New Zealand region and will contribute to understanding of the opening mechanisms of continental rifts worldwide.

[6] Rift processes and elements of extension models (e.g., successive uniform stretching and simple shear) can be tested by means of deep crustal seismic surveys and potential field methods. To investigate the mechanisms of the Bounty Trough opening and its role in the early development of the southwest Pacific, the Alfred Wegener Institute for Polar and Marine Research (AWI), the Institute of Geological and Nuclear Science (GNS), and Macquarie University conducted deep penetrating seismic and potential field experiments (CAMP project) across the Campbell Plateau and the Bounty Trough. This paper focuses on the combined gravity, multichannel reflection, and refraction/wide-angle reflection seismic transect, AWI-20030002, running north-south across the Middle Bounty Trough at 177.5° E (Figure 1). Our findings define the prerift size of the Campbell Plateau/Chatham Rise and thus help to further constrain reconstructions of the late Gondwana breakup.

1.1. Geological Setting

[7] The Bounty Trough is a Cretaceous rift feature according to Krause [1966] and Carter *et al.* [1994], interpreted by Davy [1993] as a feature of back-arc extension. It was formed during the late stages of Gondwana

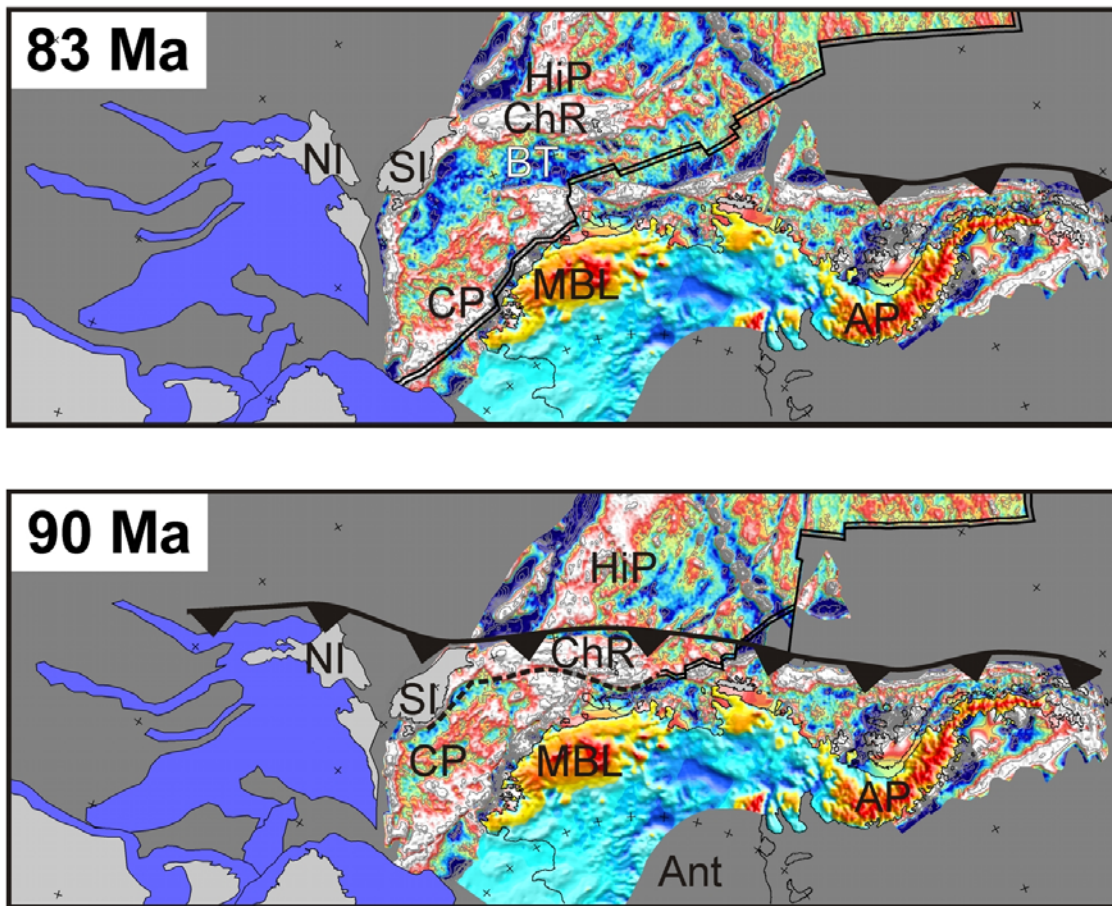


Figure 2. Two time slices from the reconstruction of the opening of the southwest Pacific in the late Cretaceous, after *Eagles et al.* [2004]. (bottom) Campbell Plateau and Chatham Rise are still parts of the same submarine plateau prior to 90 Ma. The black line marks the fossil subduction zone of the Phoenix Plate beneath the Chatham Rise, and double lines indicate active extension or seafloor spreading. Dashed black line is the future Bounty Trough axis. (top) At 83 Ma the Bounty Trough has opened, while Campbell Plateau is still attached to Marie Byrd Land. The reconstruction includes offshore free-air gravity anomaly data [*McAdoo and Laxon, 1997; Sandwell and Smith, 1997*] and data from the BEDMAP compilation for onshore Antarctica [*Lythe et al., 2000*]. Blue and green colors indicate negative free-air gravity values; orange, red, and white colors indicate positive free-air gravity anomalies. Areas not included in the modeling process, or subducted areas, are shaded in solid gray. Abbreviations are Ant: future Antarctic plate, AP: Antarctic Peninsula, BT: Bounty Trough, CP: Campbell Plateau, ChR: Chatham Rise, HiP: Hikurangi Plateau, MBL: Marie Byrd Land, NI: North Island of New Zealand, and SI: South Island of New Zealand.

breakup [*Eagles et al., 2004*]. Running east-west for ~ 1000 km and with a width of ~ 350 km, the trough separates the Chatham Rise in the north from the Campbell Plateau with its northeastern part, the Bounty Platform.

[8] Bounty Trough deepens toward the Pacific Ocean in a series of broad terraces [*Davey, 1977*]. Two ca. 1 km high basement steps [*Carter et al., 1994*] separate the Bounty Trough into three subbasins. The steps can only be distinguished in bathymetry data (Figure 1), and give rise to no gravity anomalies in the satellite data (Figure 3). The prominent Bounty Channel, one of the world's major drainage channels, cuts deeply into the sediment fill along the axis of the Bounty Trough [*Carter and Carter, 1987*].

[9] The timing of the Outer Bounty Trough opening is relatively well known: A linear magnetic anomaly immedi-

ately south of the Chatham Islands has been associated with oceanic crust. This anomaly might be the young end of anomaly 34, formed during the earliest seafloor spreading (~ 83 Ma) between Marie Byrd Land and New Zealand [*Davy, 1993, 2006*]. *Carter et al.* [1994] postulated that the basal sedimentary unit (D1) in the Outer Bounty Trough might be as old as early Cretaceous. East-west trending mid-Cretaceous faults define the margin between Chatham Rise and the Bounty Trough. These faults imply a similar age of initial faulting and sedimentation in this region [*Laird, 1993*], too. *Wood and Herzer* [1993], using seismic data from the Chatham Rise area, interpreted Bounty Trough rifting as having ceased in late Campanian times (83.5–71.5 Ma). This is later than in a recent plate tectonic reconstruction [*Eagles et al., 2004*], where the opening of

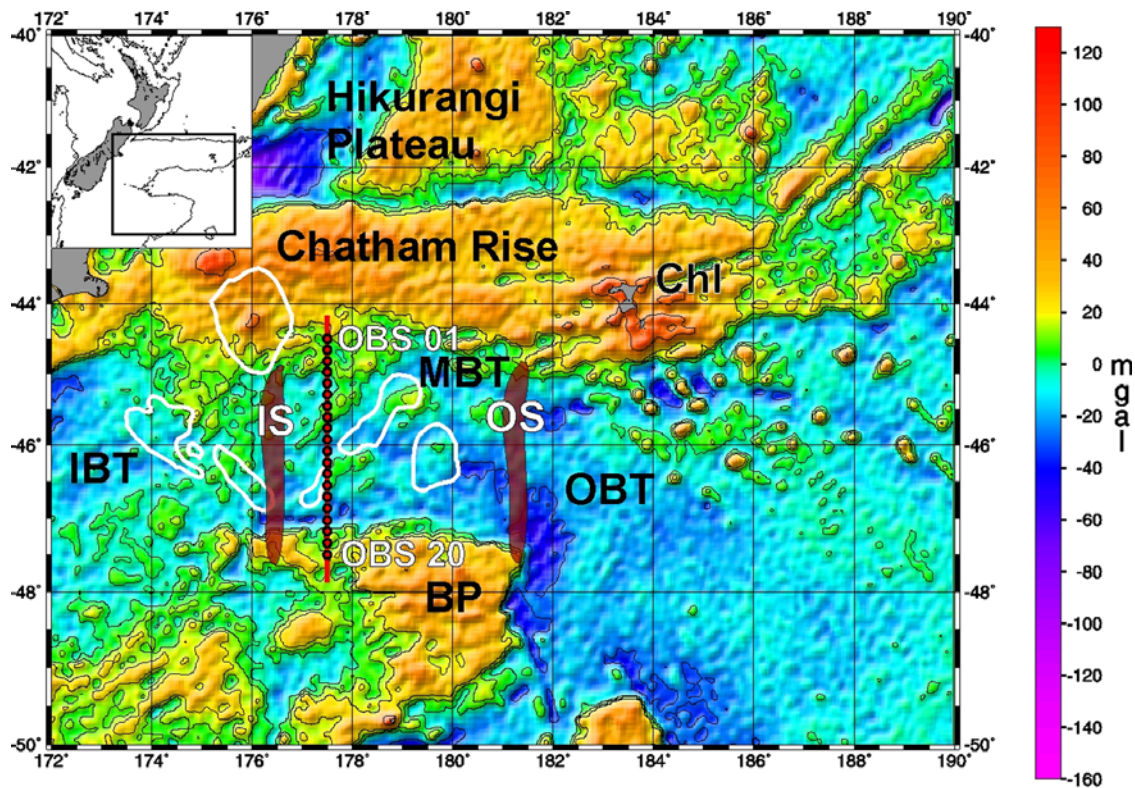


Figure 3. Satellite gravity anomaly map [Sandwell and Smith, 1997] of the Bounty Trough. Contour intervals are 20 mgal. Gravity lineaments trend at N45E, an angle of 45° to the Bounty Trough axis. In the Middle Bounty Trough, regional gravity anomalies match magnetic anomalies (white outlined areas, after [Sutherland, 1999]), while anomalies in the Inner Bounty Trough do not. The red line indicates profile AWI-20030002, and the black circles mark the positions of the ocean bottom seismographs (OBS). IBT: Inner Bounty Trough, MBT: Middle Bounty Trough, OBT: Outer Bounty Trough, BP: Bounty Platform, ChI: Chatham Islands, IS: Inner Sill (basement step), and OS: Outer Sill (basement step).

Bounty Trough occurs prior to 83 Ma. On the basis of an investigation of the Otago Schist, Forster and Lister [2003] proposed two phases of extension in the eastern New Zealand region during the Cretaceous. A first phase occurred parallel to the margin of Gondwana at ca 115 Ma. At ca 110 Ma, extension rotated by approximately 90°, perpendicular to the Gondwana margin. Following the ideas of Bradshaw *et al.* [1996], Forster and Lister [2003] suggested that extension of the Bounty Trough occurred at ca 115 Ma and lasted until ca. 85 Ma. The zone of crustal extension is suggested to have continued across the then South Island of New Zealand.

[10] Davy [1993] identified a set of quasi-symmetric magnetic anomalies that are aligned approximately parallel to the axis of Bounty Trough. The source rocks of these anomalies lie within the basement, which was suggested to consist of Permian to Triassic ocean crust because the onshore continuation of the anomalies lies in the Permian Dun Mountain Ophiolite Belt [Carter *et al.*, 1994]. On newer maps of magnetic anomaly intensity in this region, the linear nature of individual anomalies within the Bounty Magnetic Anomaly System is not so distinct [Sutherland, 1999]. A moderate correlation with some gravity anomaly structures, as seen in the satellite altimetry derived data set [Sandwell and Smith, 1997], suggests that the Bounty Trough magnetic anomaly pattern does not represent a

remanent magnetization caused by field reversals. However, the magnetic anomalies in the Bounty Trough do raise the question of whether Bounty Trough opening followed any preexisting Permian structure [Davy, 1993]. Alternatively, the magnetic anomalies might be related to Cretaceous igneous activity [Sutherland, 1999].

[11] In the Middle Bounty Trough, sediments are underlain by highly fractured basement structures [Davey, 1977]. A block-faulted basement floors the Inner Bounty Trough. Cretaceous half-grabens face north within the basement of the Inner Bounty Trough [Wood and Herzer, 1993] in a 100 × 100 km area south of the trough axis near 174°E [Davy, 1993]. Elsewhere, wherever half-grabens are observed, they face dominantly to the south. East of 178.5°W, Davy [1993] has interpreted oceanic crust. Additional information about the crustal structure of the Bounty Trough can be inferred from examination of the crust of the adjacent plateaus, Chatham Rise and Bounty Platform. Chatham Rise is a submerged continental plateau, whose basement consists of Upper Paleozoic and Mesozoic schists and greywackes of the Torlesse Terrane [Adams and Robinson, 1977; Bradshaw *et al.*, 1981]. Dredged samples from near the Bounty Islands, on the Bounty Platform, are comparable with early Paleozoic metasedimentary rocks (e.g., Greenland Group) [Beggs *et al.*, 1990]. The Bounty Islands themselves are mostly composed of Early Jurassic

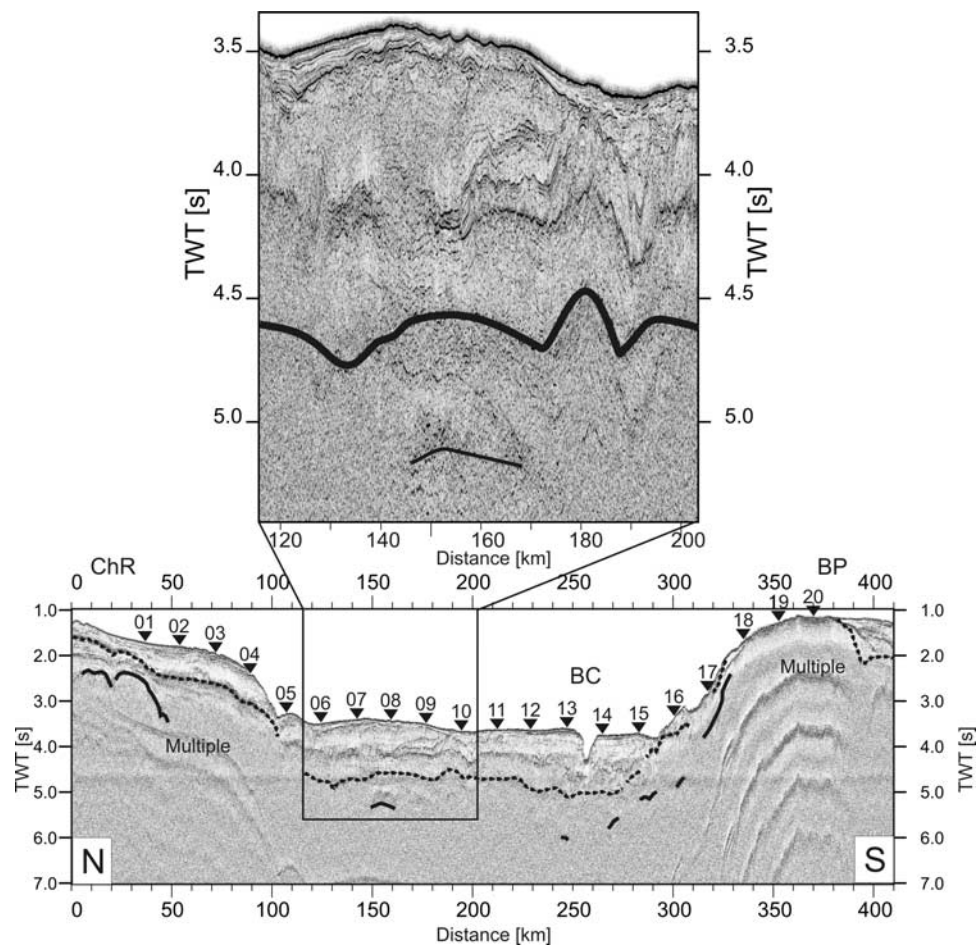


Figure 4. Stacked multichannel seismic line AWI-20030002 across the Bounty Trough. Black solid line indicates the tentatively interpreted top of crystalline basement; the black dashed line marks the acoustic basement below stratified sedimentary layers. Triangles and numbers indicate the OBS locations along the transect.

granodiorites correlative to the Median Tectonic Zone (Median Batholith) [Beggs *et al.*, 1990; Kimbrough *et al.*, 1994]. Bradshaw [1991] supposed, from geological evidence, that the preopening crustal thickness of the present northern Campbell Plateau might have been approximately 40 km.

1.2. Data Acquisition and Processing

[12] Line AWI-20030002 of the CAMP experiment is a 410 km long transect crossing the Bounty Trough from the Campbell Plateau to Chatham Rise. Along this line, we acquired a combined refraction/wide-angle reflection and multichannel seismic (MCS) data set (Figure 1). The receiver arrays were a single 2150 m long streamer, and 20 GEOPRO ocean bottom seismographs (OBS) equipped with three-component 4.5 Hz geophones and a hydrophone. An array of six G-Guns[®], with a total volume of 48 l (2980 in³) [Gohl, 2003] generated the signals. OBS stations were spaced at ~17.5 km intervals; shot spacing was approximately 150 m. Bathymetry and water depths along the profile were recorded with R/V *Sonne's* onboard SIMRAD[®] EM-120 and Parasound systems. We converted the OBS data to SEG Y format and applied corrections for the drift of the OBS clock. Exact OBS along

track positions at the seafloor were relocated using direct wave arrivals. The maximum horizontal distance between an OBS deployment location and its position on the seafloor was 280 m.

[13] To enhance the signal-to-noise ratio, the data were filtered with a time- and offset-dependent band-pass filter, deconvolved with a 200 ms spiking deconvolution, and FK filtered at large-offset ranges to suppress wraparound noise from previous shots. After each of these processing stages, we picked seismic phases. The resulting picks were carefully compared with each other for the highest signal-to-noise ratio data in order to exclude phase shifts caused by any of the three processing steps.

[14] Multichannel seismic data were processed in a standard processing stream comprising sorting (50 m common-depth-point (CDP) interval), a detailed velocity analysis (every 50 CDPs), multiple suppression via a Radon transform, spike deconvolution to remove the bubble effect, corrections for spherical divergence and normal moveout, residual static corrections, stacking, and post-stack time and depth migration with an emphasis on enhancing of deep reflections. Further details of the processing and interpretation of these multichannel seismic reflection lines are given by G. Uenzelmann-Neben *et al.* (Neogene sediment structures in Bounty Trough, eastern New Zealand: Influence

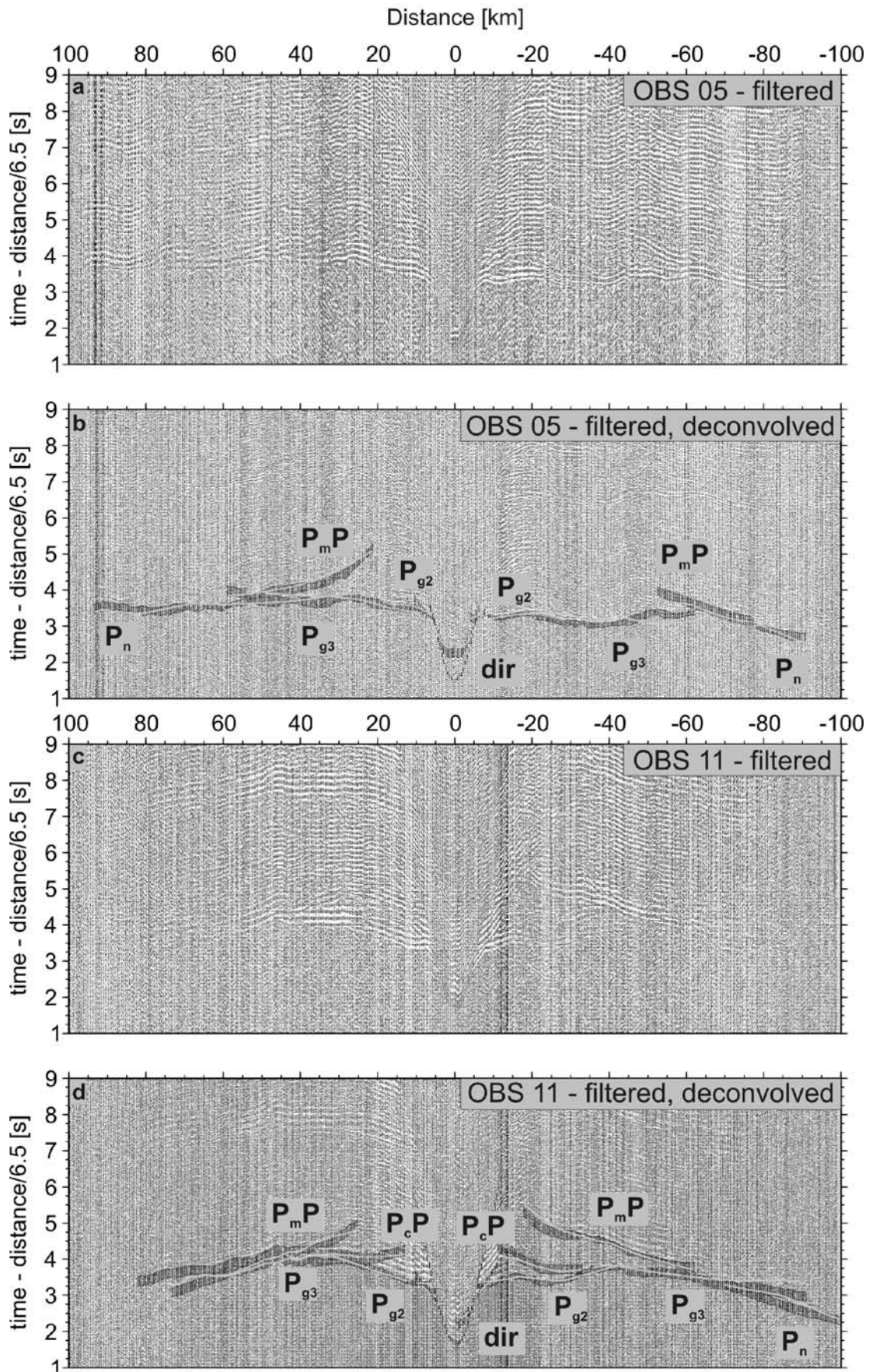


Figure 5

of magmatic and oceanic current activity, submitted to *GSA Bulletin*, 2006; hereinafter referred to as G. Uenzelmann-Neben et al., submitted manuscript, 2006).

[15] We obtained free-air gravity anomalies from a shipboard LaCoste and Romberg S-80 gravimeter recorded at 1-s intervals. The measured values collected by the gravimeter are tied to the N. Z. Potsdam system (1959) via the gravity base station in Lyttleton, New Zealand.

2. Data Description

2.1. Reflection Seismic Data

[16] The seismic reflection data show a thick stratified fill (up to 2000 m) (Figure 4) in the Bounty Trough. A strong reflector marks the bottom of the stratified layers. This transition to acoustic basement is visible in most of the MCS profile (G. Uenzelmann-Neben et al., submitted manuscript, 2006). Only a few discontinuous reflective patches can be seen beneath the acoustic basement reflector. The internal structure of this interpreted basement is poorly defined in the trough. Moho cannot be observed anywhere in the reflection seismic data.

2.2. Refraction Seismic Data

[17] The vertical component of the OBS data record shows coherent P-wave phases at up to 120 km offset (Figures 5 and 6). S-wave phases can be seen in the horizontal components of the OBS data at up to 70 km offset, with a lower signal-to-noise ratio than the vertical component recordings (Figures 7 and 8). P-wave sections (Figure 5) consistently show high-amplitude wide-angle reflections from the Moho (P_mP). A few records contain intracrustal reflections of low amplitude (P_cP). An example of the P_cP -phase is displayed for OBS 05 (Figure 5d).

[18] We identified refraction arrivals from two layers above and two layers below the acoustic basement. However, an exact separation into different crustal phases was impossible because of the strong influence of topography in the records. Apparent velocities of phases traveling through the middle and lower crust beneath the Bounty Channel are distinctly higher than the average apparent velocity over all stations, whereas phases traveling through the crust of the Bounty Platform are slower. On some of the OBS records, we observed weak P_n phases (refractions within the uppermost mantle) (Figure 5).

[19] Horizontal component sections suffer from strong ringing and are thus of lower quality. However, a sufficient number of records show crustal refraction phases (S_g) (Figure 7) and reflections from the Moho (S_mS). Because of interfering P- and S-phases at small offsets (<12 km), it was impossible to detect refractions from the sediment layer.

3. Seismic Traveltime Modeling

[20] We applied a layer-stripping procedure to refine the velocity-depth model by forward modeling. The MCS

profile provided boundary conditions for the seafloor and acoustic basement depths. The forward modeling was followed by a successive traveltimes inversion [Zelt and Smith, 1992] to fine-tune the model, using all P-wave reflected and refracted phases. At this stage we only allowed positive velocity gradients. As only very few shallow wide-angle reflections can be seen in the data, the top of acoustic basement taken from the MCS was retained. Another velocity interface was introduced into the middle crust of the model to provide a change in the velocity gradient only. Intracrustal reflections (P_cP) associated with this interface, were recorded by only one OBS (station 16, Figure 6).

3.1. P-Wave Modeling

[21] While the resolution of the velocity-depth model (Figure 9) can be calculated within the inversion scheme [Zelt, 1999], it is more difficult to quantify errors in phase identification and discrimination. Therefore we set the pick uncertainties from 40 ms to up to 125 ms depending on the signal-to-noise ratio [Zelt and Forsyth, 1994]. Although the true pick uncertainty might be lower than the assigned pick uncertainty, an estimate of the uncertainty in correct phase identification is included with this value [Berndt et al., 2001].

[22] The traveltimes inversion process helps assess the model quality as it calculates rms errors, model-based traveltimes, and Chi-squared values for each branch of the traveltimes curves (Table 1). With the uncertainties presented above we calculated traveltimes residuals and normalized Chi-squared values. These values accompanied by the number of picks are presented in Table 1. The overall rms misfit is 0.138 s with a normalized Chi-squared value of 1.972, which is close to the optimum of 1. Figure 10 presents the values of the main diagonal of the resolution matrix of the P-wave velocity depth model. Maximum resolution is represented by a value of 1. Smaller values denote a spatial averaging of the true earth by a linear combination of model parameters [Zelt, 1999]. Resolution matrix values greater than 0.5 indicate well resolved nodes.

[23] Our P-wave model is best resolved (Figure 10) in the upper and lower crust over the range of the complete Bounty Trough and main parts of the Bounty Platform and Chatham Rise, where ray coverage is densest. As more rays turn in the upper part of a layer, this part is generally better resolved than the lower part of the layer. A reasonable (0.5–0.6) resolution is calculated for the uppermost mantle in the central part of the Bounty Trough. A change in the geometry of the Moho, and limited offsets, did not allow recording P_n phases at the flanks of the trough. Many regions of the velocity model are less well resolved for the sediment layers. Because of smaller offset ranges and the masking effect of high-amplitude direct wave arrivals [White and Matthews, 1980] upper parts of the model are less covered with overlapping rays. Structural uncertainties in the upper layers are reduced by reference to the coincident MCS line. Intracrustal layer boundaries are not well

Figure 5. Sample sections of vertical components of OBS records from stations 05 (top) and 11 (bottom). All sections are plotted with a reduction velocity of 6.5 km/s applied. Sections are (a and c) filtered and (b and d) deconvolved and filtered. Each lower section (Figures 5b and 5d) shows picked and calculated traveltimes; the size of the error bars indicates the assigned pick uncertainty. Light gray lines are modeled traveltimes.

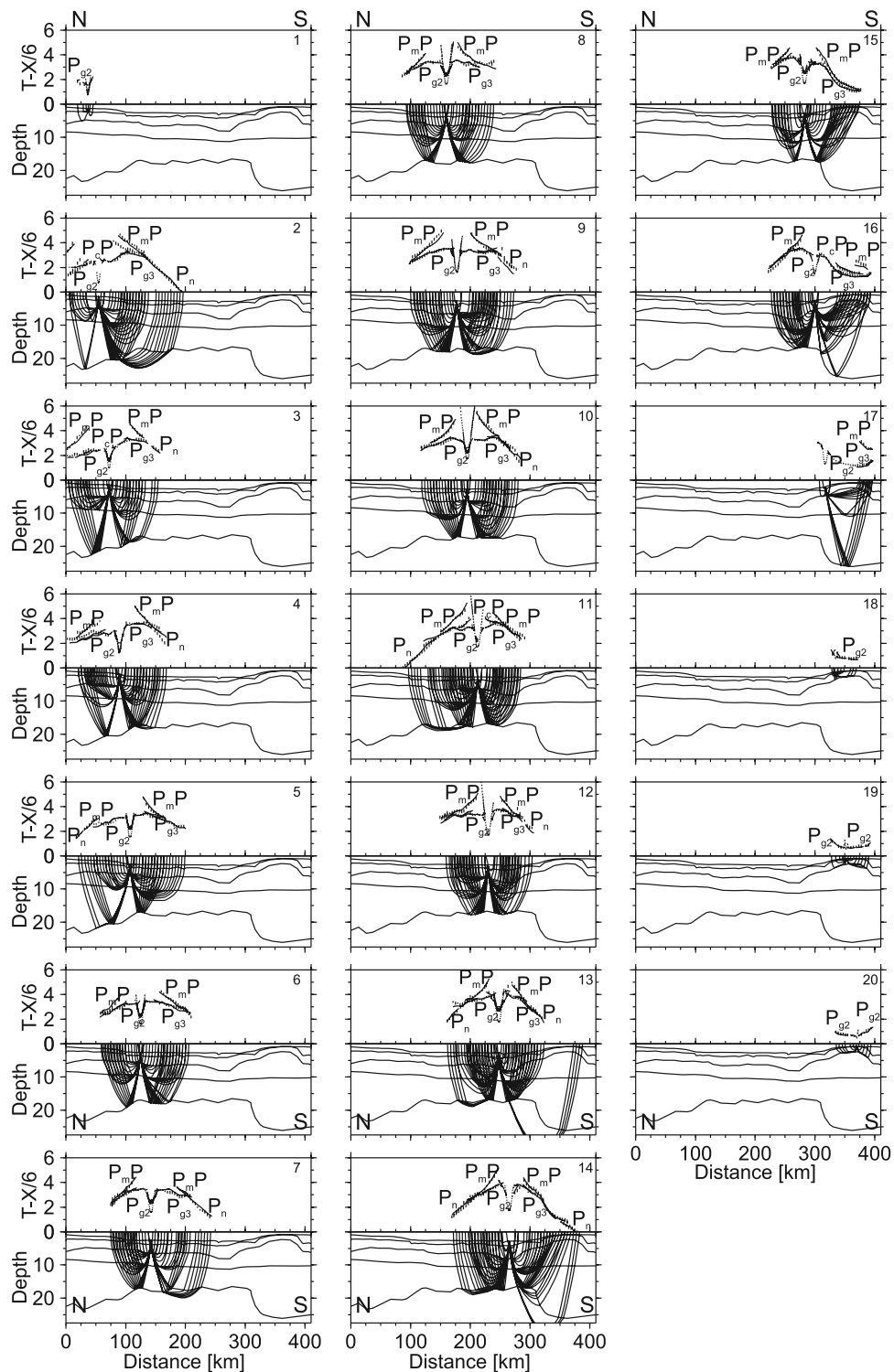


Figure 6. Comparison of picked and computed traveltimes from the final P-wave model for each vertical component of an OBS station combined with the corresponding ray paths. OBS locations are given in Figure 4. Depth in km, T-X/6 in s. Traveltimes are plotted with a reduction velocity of 6 km/s. Vertical error bars indicate observed times; the size of the bars corresponds to the assigned pick uncertainty. Calculated traveltimes are shown as solid lines. Near-offset phases (P_{g1} , P_{scd} , direct wave) are not labeled.

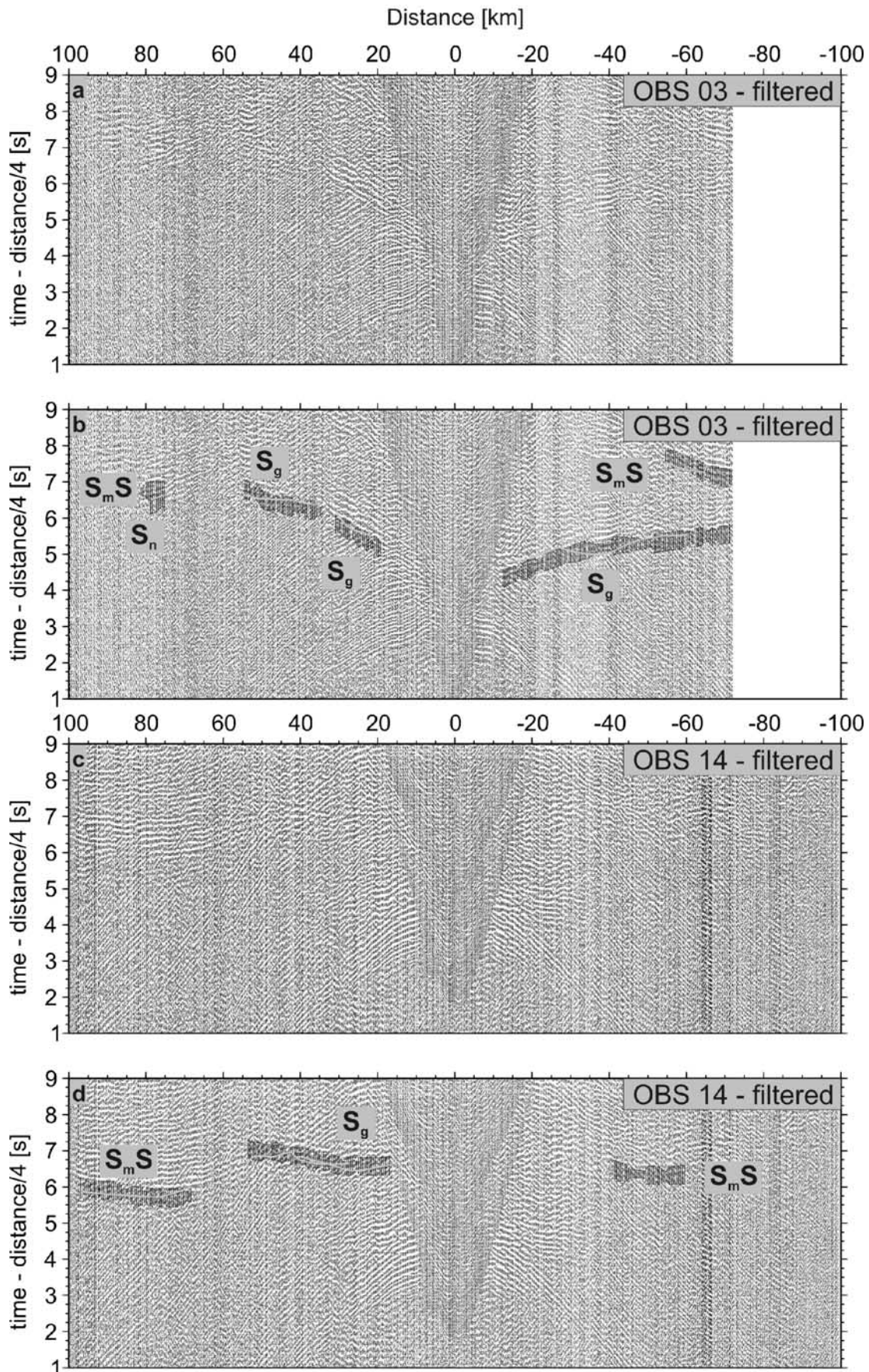


Figure 7

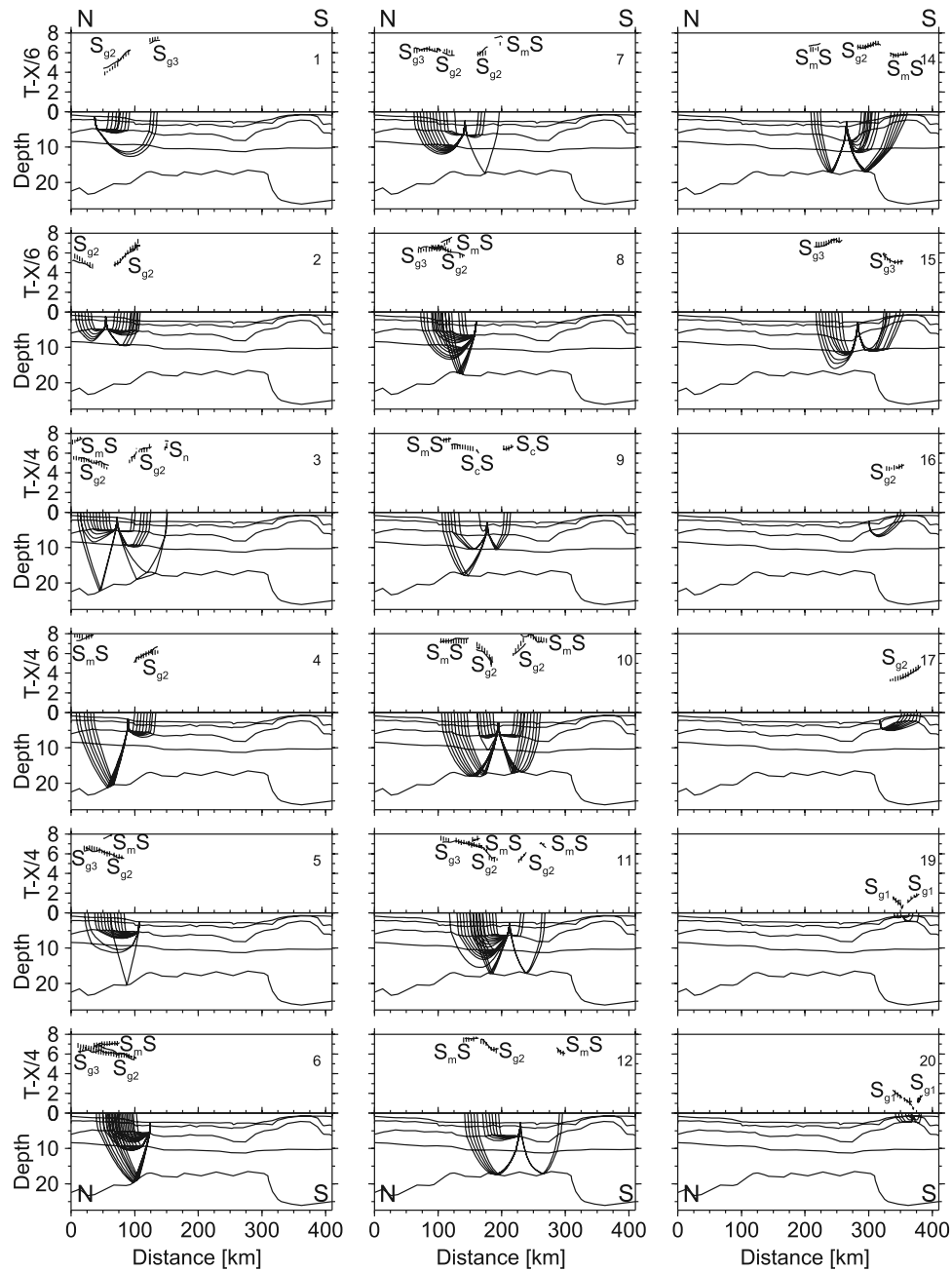


Figure 8. Comparison of picked and computed traveltimes from the final S-wave model for each horizontal component of an OBS station combined with the corresponding ray paths. No coherent S-wave energy could be observed at stations 13 and 18. Traveltimes are plotted with a reduction velocity of 4 km/s. Depth in km, T-X/4 in s. Vertical error bars indicate observed times; the size of the bars corresponds to the assigned pick uncertainty. Calculated traveltimes are solid lines.

resolved, but they were introduced to allow for changes in velocity gradient. In contrast to the intracrustal interfaces, the Moho is very well resolved because of a high number of P_mP phases. 91% of the nodes have resolution values greater than 0.90, 82% values greater than 0.97.

3.2. S-Wave Modeling

[24] For this model (Figure 11) we assigned the same layer interfaces as in the P-wave model, assuming that the observed P- and S-wave energy was generated at the same seismic boundaries and that anisotropy is negligible

Figure 7. Sample sections of horizontal components of OBS records from stations 03 (top) and 14 (bottom). All sections are plotted with a reduction velocity of 4 km/s applied. Sections are filtered. (b and c) Sections show picked and calculated traveltimes; the size of the error bars indicate the assigned pick uncertainty. Light gray lines are modeled traveltimes.

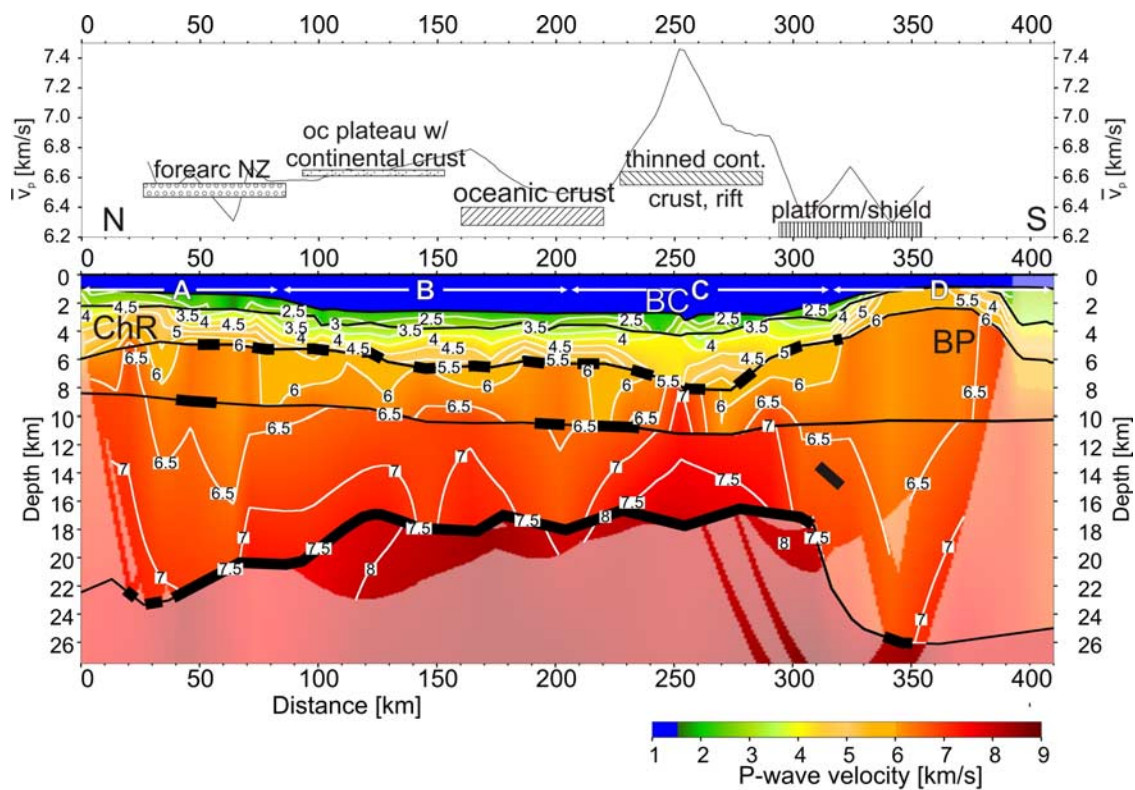


Figure 9. Final P-wave velocity-depth model overlain by a semitransparent mask in areas without ray coverage. (top) Average crustal P-wave velocities in regions with ray coverage down to the Moho. The bars superimposed to the average crustal velocities show average crustal velocities for comparable crustal regions calculated from values of the CRUST2.0 model [Bassin *et al.*, 2000]. Bold sections of layer interfaces are constrained by wide-angle reflections. A high number of very short sections constrained by reflections are marked by the bold dashed layer interface interpreted as top of basement. Abbreviations are BC: Bounty Channel, BP: Bounty Platform, and ChR: Chatham Rise. Regions A–D span (A) Chatham Rise, (B) northern Middle Bounty Trough, (C) southern Middle Bounty Trough, and (D) Bounty Platform.

[Musacchio *et al.*, 1997]. We derived an initial S-wave velocity model by converting P-wave model velocities to S-wave velocities using constant Poisson's ratios for each individual layer. Most of the layers were converted with a standard value of 0.25, but for the sedimentary layer a value of 0.38 was used to allow for the significantly lower S-wave velocities in sediments [Digranes *et al.*, 1998]. Subsequently, we started a forward and inversion process analogous to the P-wave modeling using S_g and S_mS phases picked in the horizontal component sections. During these processes we only allowed the velocity nodes to vary in value.

[25] Because of a low signal-to-noise ratio for S-wave phases we assigned pick uncertainties up to 250 ms. Therefore we allowed for an increased ambiguity in the phase discrimination because of interference and possible intrabed multiples. The number of interpreted S-wave phases is considerably smaller than the number of P-wave phases, resulting in fewer and smaller well-resolved areas (Figures 6 and 8) and an increased rms-misfit (Table 2). The overall rms residual is 0.216 s with a normalized Chi-squared value of 1.334. In general, poorly resolved regions in the P-wave model have even worse resolutions in the S-wave model, whereas regions with a high resolution in

the S-wave model also are well resolved in the P-wave model (Figure 12). In particular, the upper crust and the lower sedimentary layer in the northern Bounty Trough (50–220 km) exhibit high to very high resolution values (0.6–1.0). The upper crust of the Bounty Platform (320–370 km) is also well resolved. However, the upper crust beneath the Bounty Channel and the sedimentary layers have a low resolution; here poor data quality is likely due to interference within the wave field and energy loss due to phase conversion at the seafloor. With only very few exceptions the only observed reflection phases are S_mS phases. Resolution values of the parts of the Moho covered by S_mS reflections lie mainly above 0.75. The S_mS phases can be fit very well using the Moho depth taken unchanged from the P-wave model. This fact adds additional confidence to the P_mP phase modeling results.

3.3. Poisson Ratio Model

[26] The Poisson's ratio (σ) is an expression of the ratio v_p/v_s . σ is strongly influenced by the mineralogy of rocks, in particular by the amount of plagioclase feldspar ($\sigma = 0.30$) and quartz ($\sigma = 0.09$), while pressure and temperature have only minor influence [Christensen, 1996]. In order to derive a model of σ (Figure 13) from the P- and S-wave model, we kept the number of velocity and depth nodes in

Table 1. Statistics of Linear Traveltime Inversion for All Phases Within a Particular Modeling Layer of the P-Wave Velocity-Depth Model^a

Phase	t_{rms}	Chi-squared	Number of Picks
P _{sed,1}	0.147	5.650	64
P _{sed,2}	0.111	2.569	478
P _c P	0.166	3.048	405
P _{g,1}	0.123	1.960	2465
P _{g,2}	0.135	2.066	2565
P _m P	0.137	1.717	2626
P _n	0.193	3.069	850

^aThe water layer is not included in the statistics.

both models the same. Subsequently, we calculated σ for each single velocity node.

[27] The σ models often show a higher variability than separate v_p and v_s models. This reflects a higher sensitivity to changes in the lithology [Musacchio *et al.*, 1997] and a larger error in model parameters. Errors of 2% in both v_p and v_s can result in an error of over 9% in σ [Christensen, 1996]. Therefore we manually removed small-scale variations depending on values of adjacent nodes in the σ model. After the calculation of the σ model (Figure 13), we deleted obviously erroneous σ values (<0.20 and >0.32) in short wavelength variations. The high number of remaining reasonable values gives additional indication for the reliability of the velocity models.

4. Discussion of Seismic Models

[28] We calculated average crustal seismic velocities over those parts of the model, where the ray coverage reached down to the Moho. Seafloor topography, average crustal seismic velocity and velocity-depth models divide profile AWI-20030002 into four domains coinciding with Chatham Rise (A), the northern Bounty Trough (B), the southern Bounty Trough (C), and the Bounty Platform (D). Average

crustal P-wave velocities range mainly from 6.4–6.6 km/s for Chatham Rise and Bounty Platform (A and D) and rise to 6.85 km/s and 7.3 km/s above the high-velocity bodies in the northern and southern Bounty Trough (B and C) (Figure 9). Average crustal velocities, Moho depths, and Poisson's ratios at some positions of the profile are summarized in Table 3.

4.1. P-Wave Model

[29] The upper sedimentary layer shows minor lateral velocity variations. Here, P-wave velocities range from 2 to 3.5 km/s in up to 2 km of stratified sediments, except for the Bounty Platform, where the sediment coverage reaches only less than 100 m. Davey [1977], using unreversed sonobuoy data from the Inner Bounty Trough, reported velocities from 1.9 to 2.2 km/s for the upper sedimentary layer and 2.7 to 3.9 km/s for the lower sedimentary layer, consistent with our sediment velocities.

[30] P-wave velocities range from 3.3 to 3.8 km/s at the top of the lower sedimentary layer and 4.9 to 6 km/s at the bottom of the lower sedimentary layer with the highest values at the Chatham Rise. The situation at Bounty Platform is different with significantly higher velocities of 5.7 to 6 km/s and a low vertical gradient. There is only little control over the bottom of this layer across the Bounty Platform. It is most probable that the 5 km/s velocity line across the Bounty Platform represents the transition between sediments and basement, suggesting that basement crops out at the Bounty Platform. The layer thickness averages 3–4 km. Davy [1993] reported higher-velocity values of 5.9 to 6.5 km/s at depths of 1.5–3.5 km below the seafloor (b.s.f.) for the basement in the Bounty Trough in unreversed sonobuoy data.

[31] The upper crustal layer thickens from 3 km under Bounty Trough to 8 km beneath the Bounty Platform. This layer has the strongest lateral velocity variations: Velocities range from 5.5 to 6.5 km/s beneath the Chatham Rise (part A). In the northern Bounty Trough (part B), P-wave velocities slow down in average, at the top of the layer they

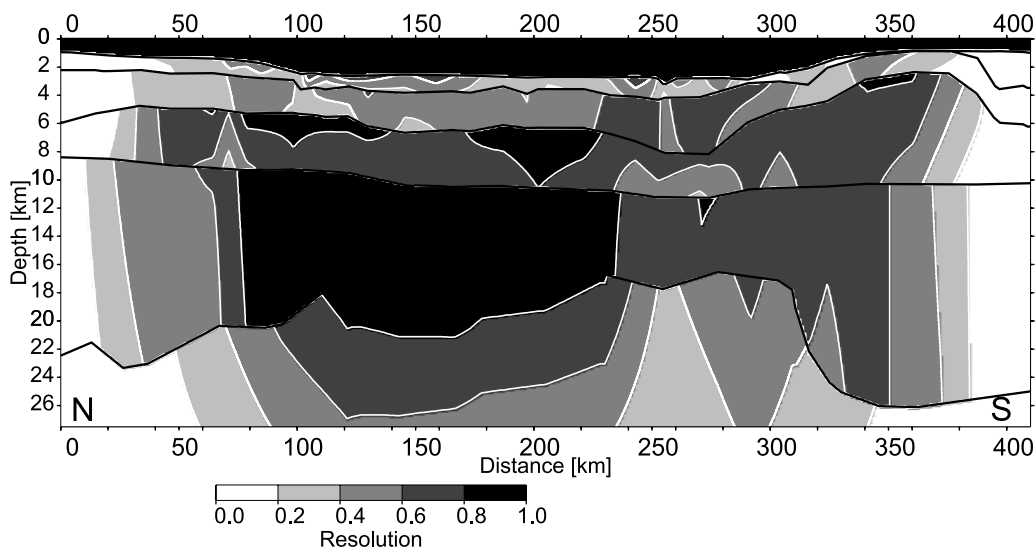


Figure 10. Resolution values calculated from traveltime inversion for the P-wave velocity-depth model. Shading corresponds to resolution values. Contour line interval is 0.2. Resolution values of greater than 0.5 indicate a moderate to good resolution.

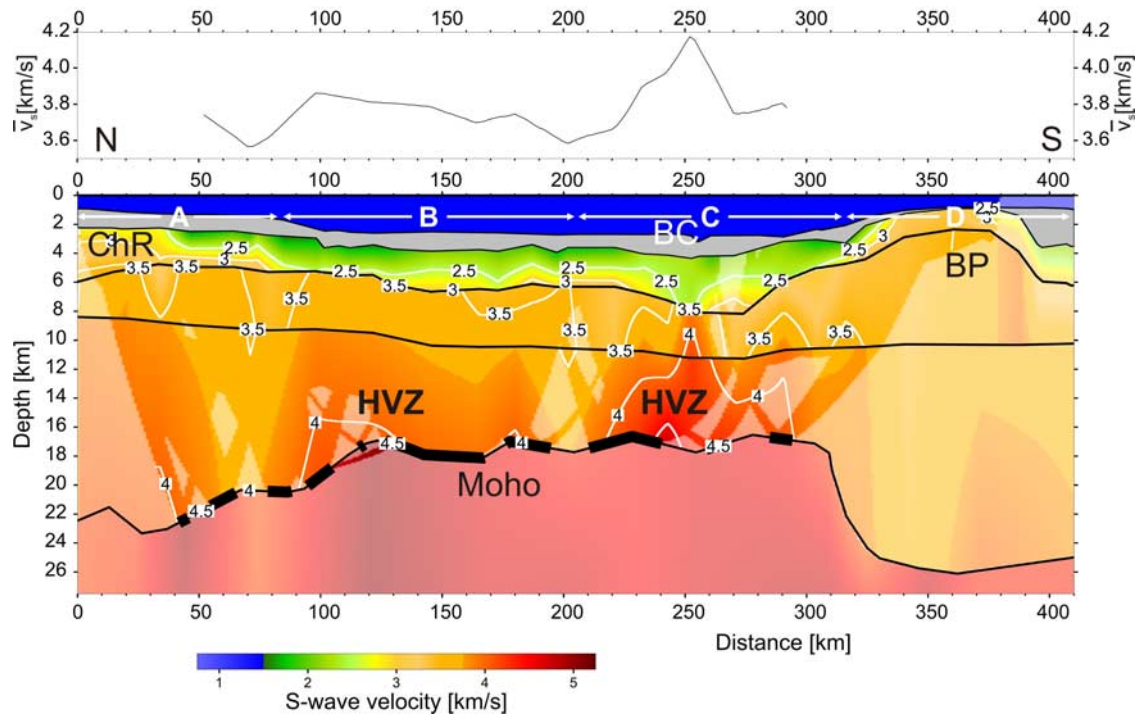


Figure 11. Final S-wave velocity-depth model overlain by a semitransparent mask in areas without ray coverage and average crustal S-wave velocities. Bold sections of layer interfaces are constrained by wide-angle reflections. Because of the significantly fewer identified S-wave phases the ray coverage and resolution are less than those of the P-wave model. Abbreviations are BC: Bounty Channel, BP: Bounty Platform, ChR: Chatham Rise.

decrease to ca. 5 to 6.0 km/s, but are nearly the same at the base of the layer. In southern Bounty Trough (part C) beneath the Bounty Channel, velocities increase to 6 to 7.2 km/s. *Davey* [1977] gave basement velocities of 5.0 to 5.6 km/s at depths of 2.5–3 km (b.s.f.) for the Middle Bounty Trough and about 6.2 km/s for the Inner Bounty Trough, which is consistent with our findings. The upper crustal velocity structure of the Bounty Platform is remarkably homogeneous, with velocities of 6 to 6.5 km/s and a low vertical velocity gradient. Generally, there is no distinct boundary between the upper and lower crust. It is merely a nonreflecting interface to allow measured gradient changes. The lower crust thins from 15 km thickness under Chatham Rise and the Bounty Platform (regions A and D) to about 6 km under the Bounty Channel.

[32] The lower crustal velocities of the Chatham Rise range from 6.2 to 7 km/s and increase to 6.8 to 7 km/s in northern Bounty Trough (part B). Further south, in the Bounty Trough, P-wave velocities increase to 7 to 7.7 km/s and slow down to 6.2 to 7 km/s beneath Bounty Platform (part D). On average, the lower crustal velocities of Bounty Trough (parts B and C) are 10 to 15% higher than those of the Chatham Rise and the Bounty Platform.

[33] The Moho can be defined by a large number of reflected phases and a few P_n phases. The entire crust thickens from 15 km under the Bounty Trough to 23 km under the Bounty Platform, and 22 km under the southern Chatham Rise. These findings agree very well with the results from gravity modeling by *Davy and Wood* [1994] who assigned a maximum crustal thickness of 23–26 km

beneath the Chatham Rise. Velocities in the upper mantle vary from 7.7 km/s to 8.2 km/s.

4.2. S-Wave Model

[34] In general, our S-wave model (Figure 11) images most of the main features of the P-wave model, while the crustal average shows only some trends. Above the high-velocity body in the lower crust of Bounty Trough (part C) the average crustal shear wave velocity rises to 4.2 km/s, but it drops to some 3.5 km/s elsewhere. Because of lower coverage, the average crustal shear wave velocity has only been calculated in regions with ray coverage down to the Moho.

[35] The upper sedimentary layer has S-wave velocities of 0.9 to 1.4 km/s, but this layer is poorly resolved, so that these values should be regarded with caution. The same can be said for the lower sedimentary layer, except on Bounty Platform (part D). Velocities in the lower sedimentary layer

Table 2. Statistics of Linear Traveltime Inversion for All Phases Within a Particular Modeling Layer of the S-Wave Velocity-Depth Model^a

Phase	t_{rms}	Chi-squared	Number of Picks
$S_{sed,2}$	0.101	0.482	84
S_cS	0.273	1.669	15
$S_{g,1}$	0.221	1.362	1524
S_cS	0.099	0.170	33
$S_{g,2}$	0.202	0.963	336
S_mS	0.243	1.729	627
S_n	0.155	0.748	8

^aThe water layer is not included in the statistics.

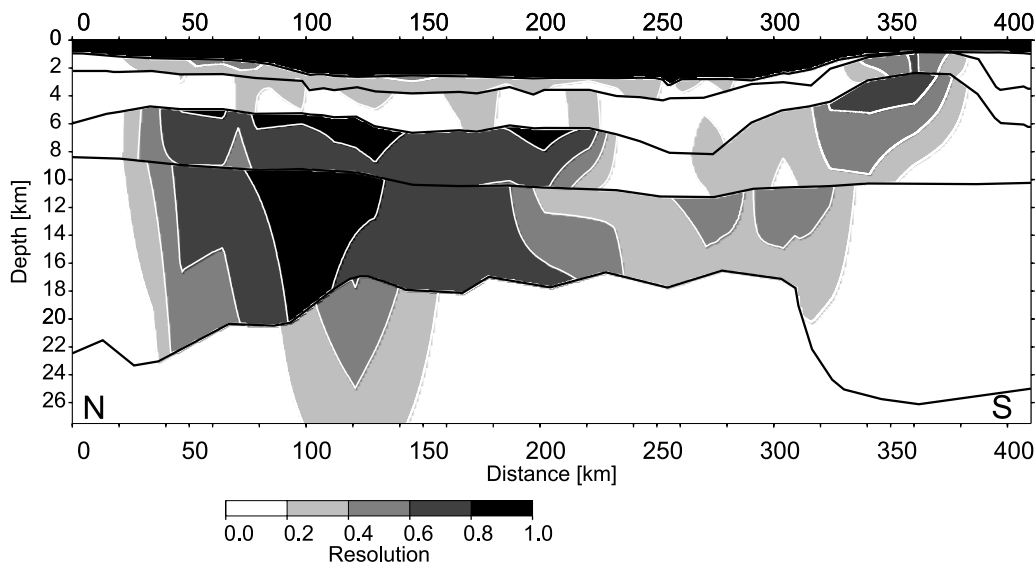


Figure 12. Resolution values calculated from traveltime inversion for the S-wave velocity-depth model. Shading corresponds to resolution values. The resolution of the P-wave model is significantly better than the resolution of the S-wave model. Contour line interval is 0.2. Resolution values of greater than 0.5 indicate a moderate to good resolution.

range from 1.7 to 3.2 km/s in Chatham Rise and Bounty Trough (parts A–C), whereas the second layer from top at the Bounty Platform has S-wave velocities from 3.3 to 3.4 km/s.

[36] S-wave velocities in the upper crust range from 3.2 to 3.6 km/s. They are homogenous throughout the complete

layer, except for a small area under the Bounty Channel, a region of the model that is poorly resolved.

[37] The lower crustal layer is the best-resolved part of the S-wave model for Chatham Rise and Bounty Trough (parts A–C); Bounty Platform (part D) is not resolved at all. Under the Chatham Rise velocities range from 3.5 to

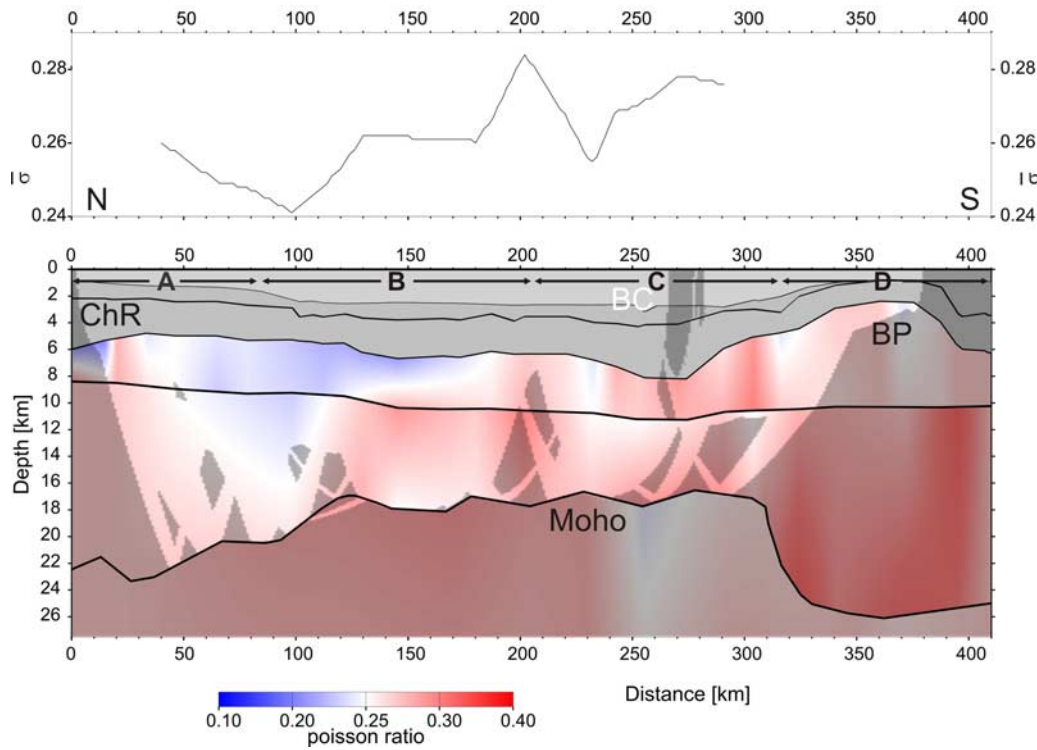


Figure 13. Poisson's ratio model and average Poisson's ratio across the Bounty Trough overlain by the semitransparent mask of the S-wave model, as the smaller ray coverage of the S-wave model determines the resolution of the Poisson's ratio model. Poisson's ratio is calculated for each node. Abbreviations are BC: Bounty Channel, BP: Bounty Platform, ChR: Chatham Rise.

Table 3. Average Crustal Velocity/ σ Values at Specific Points of the Velocity/ σ -depth Models^a

Without Sediments	50 km	90 km	125 km	250 km	290 km	350 km
σ	0.256	0.244	0.257	0.270	0.276	0.280
v_p	6.56	6.58	6.38	7.37	6.87	6.45
v_s	3.76	3.76	3.81	4.13	3.81	3.53

^aThe sedimentary layers have not been included in the calculation of the average values.

3.9 km/s and increase to 3.6 to 4 km/s under the northern Bounty Trough (part B). Southern Bounty Trough (part C) shows the highest S-wave velocities ranging from 3.9 to 4.5 km/s under the Bounty Channel.

4.3. Poisson Ratio and Crustal Composition Models

[38] As the resolution of the P-wave model is better than that of the S-wave model, the quality of the σ model (Figure 13) is mainly dependent on the S-wave model. The σ model shows some important trends. The northern part of the profile reveals low average values of σ in the crust that rise above the two zones of P-wave velocity highs. A peak, 200 km along profile, seems to result from low ray coverage at the shear wave model and a generally higher variability of the σ .

[39] In the upper crust of Chatham Rise and northern Bounty Trough (parts A and B; 50–200 km along profile), the σ is relatively low at 0.22 to 0.24. These values extend down into the lower crust of Chatham Rise (part A). In contrast, the upper crust of southern Bounty Trough and Bounty Platform (parts C and D), and the lower crust everywhere except beneath Chatham Rise have $\sigma = 0.26 - 0.30$. The highest values are found under the Bounty Channel in the upper crust and the lower crust under the whole Bounty Trough. The two sedimentary layers beneath the seafloor are poorly resolved.

[40] Individually, v_p and v_s models, or σ models are considerably nonunique when interpreted for rock compo-

sition, because many rock types have similar P-wave velocities but different σ , or vice versa [Christensen, 1996]. Nonetheless, comparisons of borehole samples with lithologies predicted by refraction velocities suggest that refraction velocities can predict regional lithological trends [Digranes *et al.*, 1996]. The nonuniqueness of σ models can be limited by comparing σ to v_p , and attempts to classify rock types by v_p and σ have enabled further constraints to be placed on the crustal composition [Christensen, 1996; Musacchio *et al.*, 1997]. The σ and v_p values, plotted in a graph for representative rock types after Christensen [1996] (Figure 14), show fields where rocks are more likely to be mafic or felsic [Musacchio *et al.*, 1997]. In order to derive a crustal compositional model (Figure 15), each corresponding pair of nodes of the crustal layers of the P-wave model and the Poisson's ratio model was plotted against the fields of rock composition (felsic/mafic). Depending on the position in the graph, a rock composition was assigned to this node and plotted in the crustal compositional model. In cases where the assignment of the crustal composition was ambiguous, the values of the adjacent nodes guided the decision.

[41] The compositional model (Figure 15) shows regions of high probability for felsic composition in most of the crust of the Bounty Trough. Three major exceptions from this observation exist in the lower crust: Our model reveals high probabilities for mafic composition in the base of the lower crust beneath Chatham Rise (part A), a portion of the base of the lower crust in northern Bounty platform (part B) and the entire lower crust and the base of the upper crust of southern Bounty Trough (part C). This mafic material in southern Bounty Trough (part C) can be correlated with the high-velocity and high-gravity bodies in the thin crust of the Bounty Trough. An area of 30% of this profile across the Bounty Trough between 50 and 325 km is strongly affected by intrusions, or about 860 km² of this cross section. We assume that 80% of this intruded material is of mafic origin [Ilchenko, 1996]. If this represents an average amount of intrusion over the entire length of

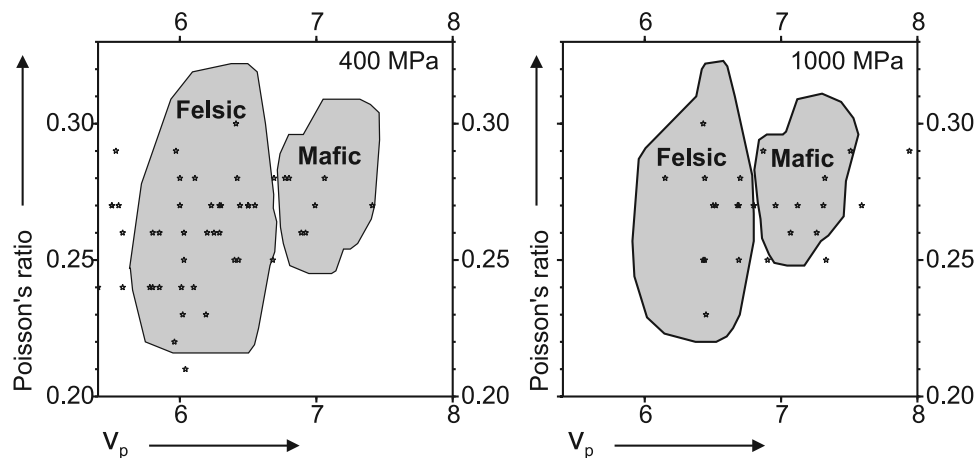


Figure 14. v_p and Poisson's ratio plotted in a combined graph. Plots show the fields of mafic and felsic rock composition for 400 MPa and 1000 MPa at middle and lower crustal depths. Gray areas of rock composition are plotted as a compilation of measurements by Christensen [1996]. Stars are values taken from the P-wave velocity and Poisson's ratio model of the Bounty Trough.

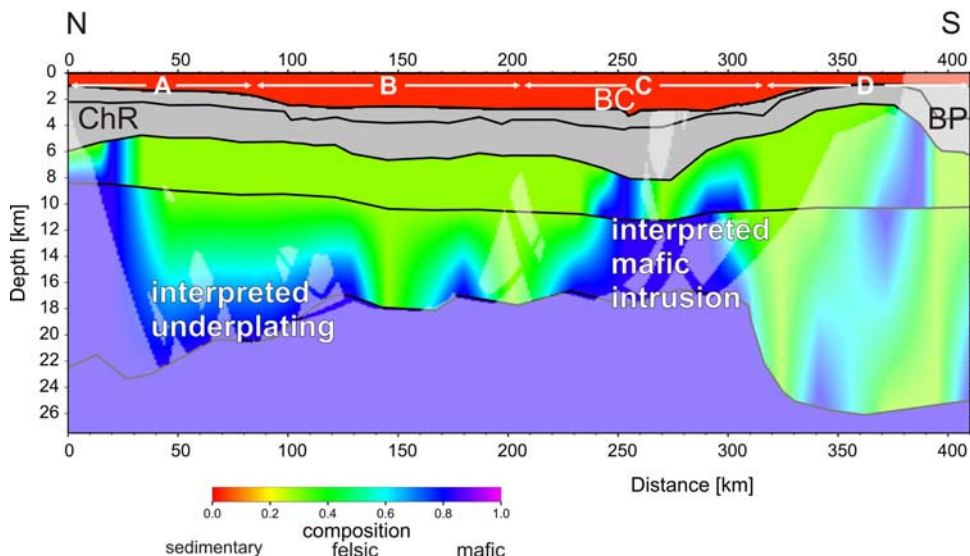


Figure 15. The compositional model shows the likelihood of rocks to consist of more felsic or mafic material depending on Poisson’s ratio and v_p . Abbreviations are BC: Bounty Channel, BP: Bounty Platform, and ChR: Chatham Rise.

Bounty Trough, the volume of intruded mafic material is around 688,000 km³.

5. Discussion of Gravity Data

[42] The gravity anomaly principally reflects the bathymetry of Bounty Trough, which, in turn, reflects crustal thinning beneath the Bounty Trough (Figure 16). The gravity model has been tied to an assumed oceanic crustal thickness southeast of Chatham Rise, and is broadly con-

strained by refraction solutions for the top and the base of the crust. Crustal thinning, as well as the deepest water depth, is concentrated in the southern Bounty Trough with a sharp increase in crustal thickness south of 300 km where the profile crosses onto the Bounty Platform. Against the broader pattern of crustal thinning in the Bounty Trough, the gravity anomaly pattern reveals structures with a wavelength of 75–100 km.

[43] A broad, ca. 25 mgal, positive anomaly centered near the axis of the Bounty Trough is partly modeled by a high-

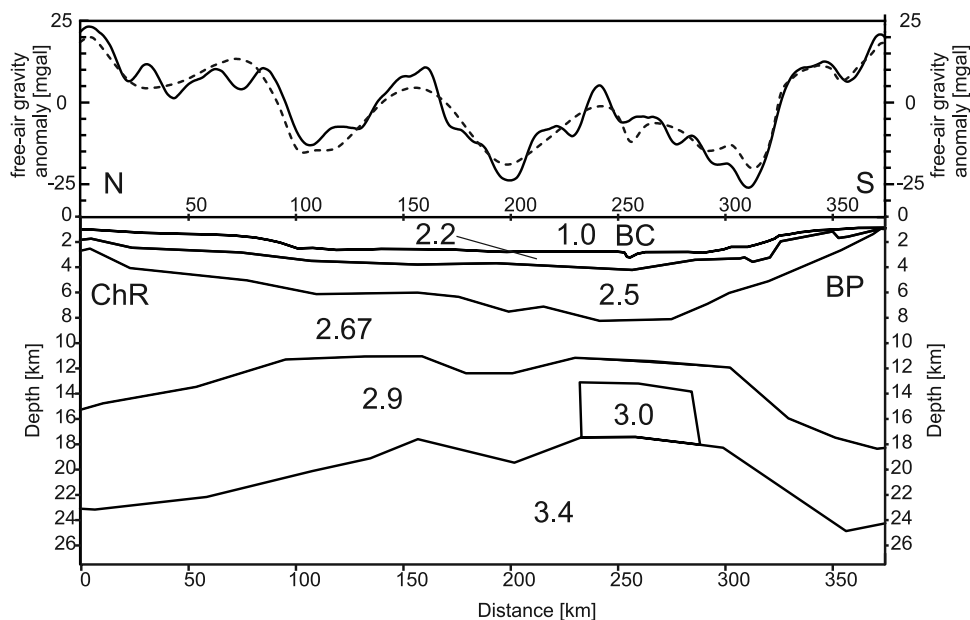


Figure 16. Minimum structure gravity model, with bodies striking orthogonal to the plane of the section and extending uniformly from each end of the section. Numbers are densities in g/cm³. Above the gravity model measured (solid) and calculated (dashed) free-air gravity anomalies are plotted. The sedimentary and crustal thickness model has been guided by the seismic refraction model. Abbreviations are BC: Bounty Channel, BP: Bounty Platform, and ChR: Chatham Rise.

density body of 3.02 g/cm^3 reaching up into the middle crustal layer against a background value of 2.9 g/cm^3 for the lower crust and 2.67 g/cm^3 for the middle crustal layer (Figure 16). Similar anomaly variations further north have been principally modeled by variations in crustal thickness. Gravity highs observed in the shipborne free-air gravity measurements correlate well with subparallel gravity lineations that can be seen in the satellite gravity data set [Sandwell and Smith, 1997]. Magnetic anomalies from marine magnetic measurements correlate well with some of the observed gravity anomalies (Figure 3), but not with others [Sutherland, 1999]. The better correlations appear in the Middle Bounty Trough, suggesting that potential field anomalies there could be attributed to mafic material intruded into the crust, whereas those in the Inner Bounty Trough may not.

6. Tectonic Implications

[44] Reflections from the Moho (P_mP and S_mS -phases), as well as the gravity model indicate a decreased Moho depth under the Bounty Trough and a strongly asymmetrical Moho topography with a steep southern flank and a gentle northern flank.

[45] The MCS section of the Bounty Trough revealed rather well stratified upper sedimentary layers and almost transparent lower sedimentary layers that appear at first glance to be upper crystalline crust at this depth. However, our P-wave velocity-depth model revealed seismic velocities of ca. $3.7\text{--}5.4 \text{ km/s}$ for this layer, too low for crystalline crust. Mortimer *et al.* [2002] observed acoustically transparent regions in the South East South Island (SESI) transect and interpreted them as weakly metamorphosed sediments (e.g., Murihiku Terrane). P-wave velocities for the Murihiku Terrane at shallow depths range from 4.7 to 5.4 km/s [Godfrey *et al.*, 2001]. Therefore we suggest a similar metasedimentary origin for the acoustically opaque zone in the Bounty Trough. The lack of stratification could be caused by periods in which the sediments have been mechanically and thermally reworked by alternating phases of extension and compression. Forster and Lister [2003] proposed the idea of a Cretaceous change in the direction of extension in the Bounty Trough. However, their model, based on the Otago Schist, does neither explain the rough topography of the acoustic basement nor the acoustically transparent layers beneath, as the compressional elements are lacking in their reconstruction.

[46] The high-velocity body, in both P-wave and S-wave seismic models at $220\text{--}280 \text{ km}$, coincides well with a high-density body in the gravity model (Figures 9 and 16). As we cannot correlate observed gravity highs with basement highs interpreted in older single channel seismic (SCS) data [Davey, 1977], we rule out basement fault blocks as the source of the gravity highs. Our compositional model shows mafic rocks reaching up into the upper crust in southern Bounty Trough (part C) and at the base of the lower crust in northern Bounty Trough (part B). In continental rift zones, very similar crustal high-velocity/high-gravity bodies have often been interpreted as mafic intrusions [Ilchenko, 1996; Keranen *et al.*, 2004]. We interpret the high-velocity body of southern Bounty Trough (part C) as a mafic body intruded into the lower and upper crust and the high-

velocity zone, further north, as possible underplating at the base of the crust.

[47] A gravity map of the Bounty Trough [Sandwell and Smith, 1997] shows several gravity lineations striking at ca. 45° to the Bounty Trough axis (Figure 3). Gravity highs and en echelon faulting in the Gulf of Aden strike at the same angle to the rift axis. Because of the position and strike direction of the gravity anomalies in the Gulf of Aden, these structures are interpreted as the expressions of magmatic cells related to incipient seafloor spreading [Dauteuil *et al.*, 2001]. Dauteuil *et al.* [2001] interpret the fact that the magmatic cells are arranged at an angle of ca. 45° to the axis of extension, as a sign of oblique rifting. We suggest that the gravity pattern in the Bounty Trough and, in turn, the mafic intrusions are comparable to those magmatic cells in the Gulf of Aden, indicating a NW-SE oblique rifting trend in the Bounty Trough.

[48] Modeled seismic velocities and crustal thicknesses (Figure 9) indicate that the Chatham Rise and Bounty Platform are composed of continental crust, consistent with outcrop and dredge samples at the Chatham Islands and Bounty Island, where rocks of the Torlesse Terrane and Greenland Group have been found [Adams and Robinson, 1977; Beggs *et al.*, 1990]. However, the seismic P-wave velocities beneath Bounty Platform and Chatham Rise are slightly higher than velocities modeled for the Torlesse Terrane in the SIGHT experiment at the eastern end of the Canterbury Basin [Van Avendonk *et al.*, 2004]. The results of the SIGHT lines [Scherwath *et al.*, 2003; Van Avendonk *et al.*, 2004] modeled the lower crust as oceanic crust, based on the consistent observations of a deep intracrustal reflector and P-wave velocities of $6.9\text{--}7.1 \text{ km/s}$, with little lateral velocity variation. The velocity information is based on a few observed turning rays only. In our models, we do not observe this deep intracrustal reflector or the homogeneous velocity layer directly above the Moho, and therefore cannot associate the oceanic crust interpreted in the SIGHT lines with the rifting event interpreted in this paper, supported by the rejection of the interpretation of oceanic crust by Mortimer *et al.* [2002].

[49] The crystalline crust thins from $21\text{--}23 \text{ km}$ at the flanks of the Bounty Trough to some $9\text{--}10 \text{ km}$ under the trough. If this crustal thickness variation is the result of crustal thinning beneath the Bounty Trough, it indicates very high stretching factors (β). As it is difficult to map the interface between the upper and lower crust, we calculated stretching factors for the entire crust. Calculated β -factors between 2.7 and 4.4 assume either an original thickness of 24 km , as observed under the Bounty Platform or 40 km as postulated by Bradshaw [1991]. A stretching factor of 3.3 is close to the value at which oceanic crust would form [Allen and Allen, 1990]. Our very high stretching factor and the fact that the interpreted magmatic intrusions reach far into the upper crust suggest that, at the location of our transect, rifting of the Bounty Trough ceased at or shortly after the onset of seafloor spreading. Depending on its timing, the location of rifting could have moved from the incipient Bounty Trough ocean to the later Campbell Plateau–Marie Byrd Land rift zone, as envisaged in the reconstructions of Eagles *et al.* [2004].

[50] Davy and Wood [1994] modeled the Chatham Rise crust as ca. 25 km thick. The crust at the margin of the

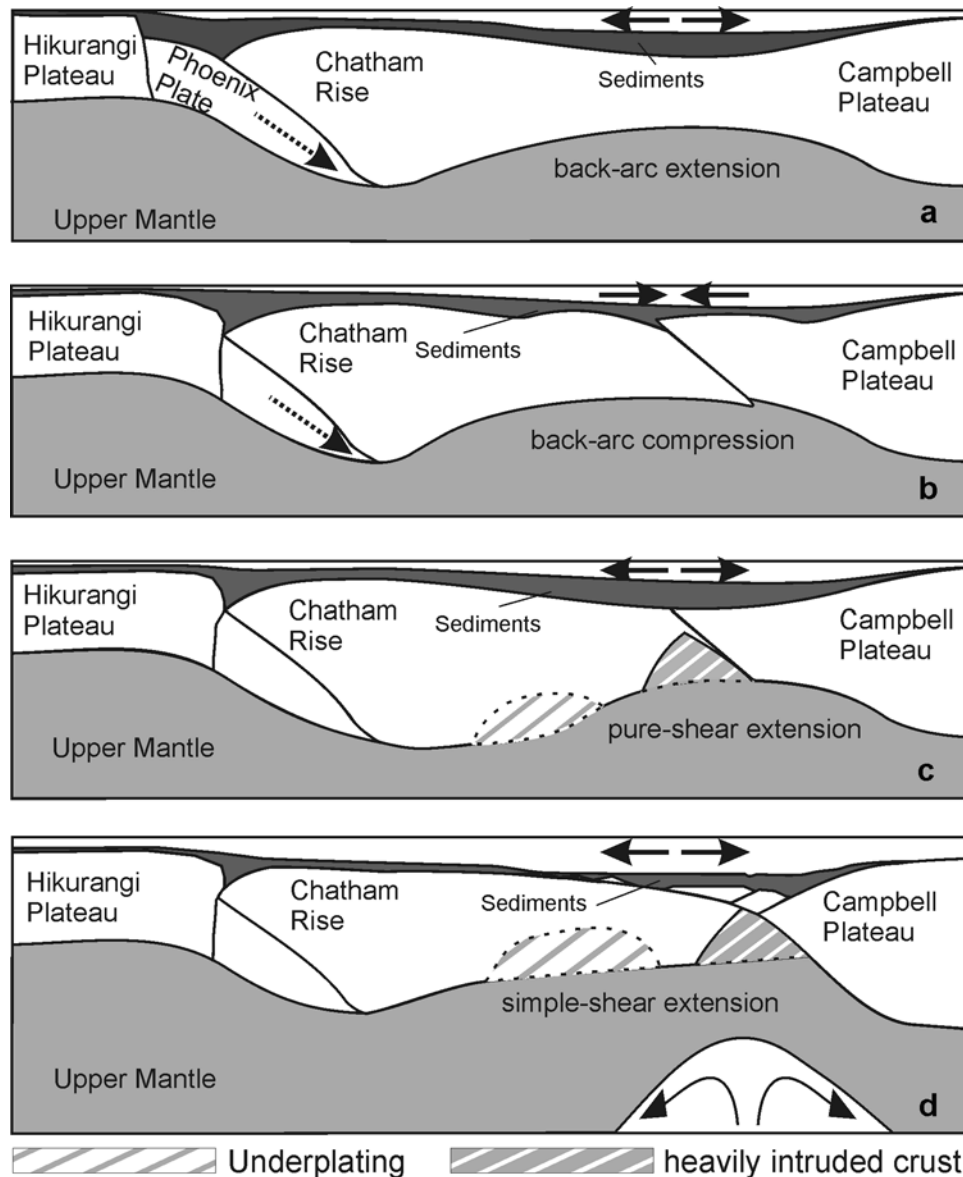


Figure 17. Evolutionary tectonic model of the Bounty Trough. Horizontal solid arrows show the direction of Bounty Trough deformation, dashed arrows show the direction of the subduction of the Hikurangi Plateau, and curved arrows indicate possible mantle flow pattern. (a) Subduction of the Pacific Phoenix Plate causes back-arc extension at Chatham Rise and Campbell Plateau. (b) The collision of the Hikurangi Plateau with Chatham Rise turns the back-arc basin into compression. At this time a weak metamorphism of previously deposited sediments occurs. (c) End of collisional phase with the beginning of extension. (d) As rifting continues, extension style changes to simple shear extension with magmatic material underplating and intruding into the crust until the onset of seafloor spreading.

Bounty Platform is about 24–26 km (this paper). Crustal thickness at the center of the Campbell Plateau is about 27 km (J. Grobys et al., paper submitted to *Tectonophysics*, 2006). Moho depth beneath the formerly adjacent western Marie Byrd Land was estimated to be at least 25–30 km [Ritzwoller et al., 2001; Luyendyk et al., 2003]. In western Marie Byrd Land, observed dikes and faults strike at a high angle to the rifted continental margin [Luyendyk et al., 2003]. The extension direction these authors recorded for Colbeck Trough, formerly adjacent to Campbell Plateau, is almost perpendicular to the direction of initial seafloor

spreading between Marie Byrd Land and the Campbell Plateau [Eagles et al., 2004]. The Colbeck Trough is attributed to intracontinental extension at 105–96 Ma [Fitzgerald, 2002; Luyendyk et al., 2003] that supposedly led to the formation of the west Antarctic and Ross Sea Rift system. From these indications, we suggest cautiously that the thinned crust of the Campbell Plateau and the Chatham Rise might be a result from the same event.

[51] The Bounty Trough lies in a setting that has been influenced by a Cretaceous and older subduction zone situated north of the Chatham Rise [Fitzgerald, 2002] and

seafloor spreading to the east (south of the Chatham Islands) (Figure 2). Both processes could have had an influence on Bounty Trough opening. *Spörl and Ballance* [1989] proposed that the early extension was the result of back-arc processes, whereas *Carter and Carter* [1987] call the Bounty Trough a failed rift arm. In this context, we use the term “rifting” only for processes at divergent margins in contrast to extensional processes related to convergent margins, here addressed as “back-arc extension”.

[52] The initial extension of a back-arc basin begins at the island arc, as it is the most ductile part of the system [*Tamaki*, 1985]. This interpretation would require the Chatham Rise to be a former island arc. The most prominent expressions of arcs are volcanic activity [*Herzer*, 1995]. Chatham Rise consists of schist and greywacke of the Torlesse Terrane [*Adams and Robinson*, 1977; *Bradshaw et al.*, 1981] rather than arc volcanic deposits, and does not seem to have been a main zone of volcanic activity [*Wood and Herzer*, 1993]. Moho depths, and the velocity distribution over the Bounty Trough show a pronounced crustal thinning, consistent with the idea of a nonvolcanic rift arm (Figure 9). The morphology of the Bounty Trough, a relatively broad sedimentary basin with steep flanks is a typical feature of an aulacogen [*Burke*, 1977]. What is more, the initiation of aulacogens is very often accompanied by the intrusion of igneous rocks [*Burke*, 1977] as indicated by high-velocity/high-density regions in the Bounty Trough.

[53] The combined interpretation of geophysical data points to an interpretation of the Bounty Trough as a failed rift arm. It cannot be ruled out that the rifting of the Bounty Trough followed preexisting zones of crustal weakness caused by the subduction of the Phoenix Plate under Chatham Rise. Sediments of the Torlesse Terrane were possibly deposited in a back-arc setting as suggested by *Davy* [1993]. Later on, they were thermally or mechanically reworked by phases of extension and compression. Albanian to Santonian (112–83.5 Ma) calc-alkaline volcanics and rhyolites, found in the Chatham Islands and South Island graben sequences, have chemistries that imply a change from a compressional to an extensional regime [*Barley et al.*, 1988]. This period of time coincides with the cessation of subduction of the Hikurangi Plateau [*Davy*, 2006]. It is possible that the subduction of the Phoenix Plate beneath the ancient Gondwana margin caused back-arc extension, as suggested by *Forster and Lister* [2003], and provided the depositional setting for pre-Cretaceous sediments in the Bounty Trough, while the collision of the Hikurangi Plateau caused the compressional forces that metamorphosed the pre-Cretaceous sediments (Figure 17).

7. Comparison With Other Rift Systems

[54] Comparisons of volcanic (Ethiopian Rift System, Red Sea, Oslo Rift) and nonvolcanic (Gulf of Aden) rift systems at the early stage of development reveal a number of processes that may have operated during Bounty Trough opening. High-velocity zones are interpreted as cooled magmatic intrusions/underplating of similar spatial extent to those in the Bounty Trough. The Oslo Rift intrusions for example are estimated to have a volume of ca. 200,000–400,000 km³ [*Pedersen and van der Beek*, 1994]. *Dugda et*

al. [2005] observed increased Poisson’s ratios similar to those in areas of the Bounty Trough in parts of the Ethiopian rift zone. They suggested that they indicate a partial modification or replacement of the crust by mafic intrusions. Local gravity highs in a regional gravity low, as found in the Bounty Trough, have been observed for example in the Dniepr-Donets Basin where they are also explained as an intrusion of magmatic and ultramafic rocks [*Yegorova et al.*, 1999]. The strong similarities in the observations mentioned above at the Bounty Trough to other rift systems confirm the notion that the Bounty Trough was a typical large rift system.

[55] Magmatic cells aligned obliquely to the direction of extension in the East African Rift System and the Red Sea [e.g., *Ebinger and Casey*, 2001] are interpreted as the loci of extension within a nascent rift system [*Dugda et al.*, 2005]. This notion can also explain the correlated gravity-magnetic anomaly patterns in the Middle Bounty Trough. In the Inner Bounty Trough crustal thinning probably occurred to a lesser extent, because here gravity anomaly patterns do not correlate with magnetic anomalies. Gravity anomaly patterns as observed in the East African Rift System or the Red Sea are absent in the Outer Bounty Trough, where oceanic crust was formed. On the basis of the comparison with the gravity patterns mentioned above, it is reasonable to interpret the gravity patterns in the Middle Bounty Trough as the expressions of magmatic cells related to incipient seafloor spreading.

[56] Evidence for large mafic intrusions in the Bounty Trough, as well as the strong structural asymmetry, do not comply well with the two end-member modes of extension. The pure shear model, where extension is distributed through the lithosphere uniformly with depth, predicts a symmetric rift architecture and crustal thinning [*Latin and White*, 1990]. In contrast, in developing an extensional model to explain structural styles in Basin and Range, *Wernicke and Burchfiel* [1982] suggested a lithosphere-scale detachment system. This model, along with other variations of simple shear extension models, can explain strong structural asymmetry across the rift. *Latin and White* [1990] found that very little magma is produced by simple shear extension. More recent studies [*Ro and Faleide*, 1992; *Louden and Chian*, 1999] have synthesized both extensional end-member models and proposed a multistage extension model that incorporates a transition from initial pure shear extension to later simple shear extension. This transitional model could well explain the rift-related features observed in the Bounty Trough, where we observe a strong asymmetry of the Moho as well as large intrusions into the crust, elements of both rift models (Figure 17).

8. Conclusions

[57] The CAMP refraction survey and subsequent modeling have revealed much about the extensional processes associated with the Bounty Trough opening. Quantification of the amount of crustal stretching and intrusion contributes to an understanding of rift processes in general and will improve plate kinematic reconstructions of the southwestern Pacific in particular. This first combined wide-angle reflection/refraction and MCS line across the Bounty Trough provides the most detailed information on deep structures of

the rift zone between Chatham Rise and Campbell Plateau. Our main results are

[58] 1. The Moho depth decreases from 24 km b.s.f. under the Bounty Platform to about 12 km b.s.f. under the Bounty Trough. It increases again to 22 km b.s.f. underneath the Chatham Rise flank.

[59] 2. Two high-velocity bodies can be observed (Figures 9 and 11) in the P- and S-wave models: A distinct 60 km wide one is situated directly under the Bounty Channel.

[60] 3. P-wave velocities in the lower crust (Figure 9) rise from 6.2–7.0 km/s beneath Chatham Rise and Bounty Platform to 7.0–7.7 km/s under the Bounty Channel and for the upper crystalline crust, from 5.5–6.5 km/s to 6.0–7.2 km/s. Lower crustal S-wave velocities (Figure 11) increase from 3.5–3.9 km/s under the Chatham Rise to 3.9–4.5 km/s beneath the Bounty Channel.

[61] 4. Free-air gravity within the regional low of the Bounty Trough (Figure 16) is characterized by anomalies of about 25 mgal amplitude and 100 km wavelength. These anomalies can be modeled by crustal thickness variations and a high-density body, which is coincident with a high-velocity body in the crust under the Bounty Channel.

[62] 5. A Poisson's ratio model (Figure 13) shows enhanced values ($\sigma = 0.25 - 0.30$) in the whole crust beneath the Bounty Channel and reduced values ($\sigma = 0.22 - 0.25$) in the crust under the northern Bounty Trough. Our compositional model (Figure 15) indicates mafic crust in the area of the pronounced high-velocity body and at the base of the lower crust of the northern Bounty Trough.

[63] All observations mentioned above support the interpretation of high-density/high-velocity bodies in the crust as magmatic intrusions into a thinned continental crust (Figure 17). We interpret the gravity patterns observed in the Middle Bounty Trough as the former locus of nascent seafloor spreading, in contrast to the Outer Bounty Trough where oceanic crust formed. The magmatic intrusions may have formed during a pure shear extension phase that was followed by a simple shear phase, which produced the overall asymmetry of the rift. Rifting ceased in the late Cretaceous. The fact that the Chatham Rise consists of continental crust, and that there are a large number of similarities in the structure and velocity distribution to modern rift systems, implies that the present Bounty Trough was not formed by back-arc extension but is a failed rift arm, which was possibly connected to a triple junction at the mouth of the Bounty Trough during the separation of New Zealand from Antarctica. However, the observation of acoustically transparent sediments suggests that an earlier process, possibly the subduction of the ancient Phoenix Plate beneath the Chatham Rise, caused back-arc extension with sediment infill until the collision of the Hikurangi Plateau with the Chatham Rise led to successive compression.

[64] **Acknowledgments.** We are grateful to the captain and crew of RV *Sonne* during cruise SO-169 for their support and assistance. This project is primarily funded by the German Federal Ministry of Education and Research under BMBF contract 03G0169A as well as through contributions from AWI and GNS. The German Academic Exchange Service (DAAD) funded a visit of J.G. to GNS for 2 months. We thank Kristina Tietze for assistance with the S-wave modeling. Furthermore, we thank GeoPro GmbH (Hamburg) for their support in providing and operating the OBS equipment and Exploration Electronics Ltd. (Norwich) for providing and operating the seismic streamer system. Graeme Eagles

and two anonymous reviewers helped to improve this manuscript. We thank Reinhard Werner, Kaj Hoernle, Fred Davey, and Nick Mortimer for fruitful discussions. Most of the figures were generated with Generic Mapping Tools [Wessel and Smith, 1998]. This is AWI contribution awi-n16038.

References

- Adams, C. J., and P. Robinson (1977), Potassium-argon age of schists from Chatham Island, New Zealand Plateau, southwest Pacific, *N. Z. J. Geol. Geophys.*, **20**, 287–302.
- Allen, P. A., and J. R. Allen (1990), *Basin Analysis, Principles and Applications*, pp. 53–91, Blackwell Sci., Malden, Mass.
- Barley, M. E., S. D. Weaver, and J. R. De Laeter (1988), Strontium isotope composition and geochronology of intermediate-silicic volcanics, Mt. Somers and Banks peninsula, New Zealand, *N. Z. J. Geol. Geophys.*, **31**, 197–206.
- Bassin, C., G. Laske, and G. Masters (2000), The current limits of resolution for surface wave tomography in North America, *Eos. Trans. AGU*, **81**(48), Fall Meet. Suppl., S12A-03.
- Beggs, J. M., G. A. Challis, and R. A. Cook (1990), Basement geology of the Campbell Plateau: Implications for correlation of the Campbell magnetic anomaly system, *N. Z. J. Geol. Geophys.*, **33**, 401–404.
- Berndt, C., R. Mjelde, S. Planke, H. Shimamura, and J. I. Faleide (2001), Controls on the tectono-magmatic evolution of a volcanic transform margin: The Vøring transform margin, NE Atlantic, *Mar. Geophys. Res.*, **22**, 133–152.
- Bradshaw, J. D. (1991), Cretaceous dispersion of Gondwana: Continental and oceanic spreading in the south-west Pacific-Antarctic sector, in *Geological Evolution of Antarctica*, edited by M. R. A. Thomson, J. A. Crame, and J. W. Thomson, pp. 581–585, Cambridge Univ. Press, New York.
- Bradshaw, J. D., P. B. Andrews, and C. J. Adams (1981), Carboniferous to Cretaceous on the Pacific margin of Gondwana: The Rangitata phase of New Zealand, in *Gondwana Five*, edited by M. M. Creswell, and P. Vella, pp. 217–212, A. A. Balkema, Brookfield, Vt.
- Bradshaw, J. D., S. D. Weaver, and R. J. Muir (1996), Mid-Cretaceous oroclinal bending of New Zealand terranes, *N. Z. J. Geol. Geophys.*, **39**, 461–468.
- Burke, K. (1977), Aulacogens and continental breakup, *Annu. Rev. Earth Planet Sci.*, **5**, 371–396.
- Carter, L., and R. M. Carter (1987), The Bounty Channel system: A 55-million-year-old sediment conduit to the deep sea, southwest Pacific Ocean, *Geo Mar. Lett.*, **7**, 183–190.
- Carter, L., and R. M. Carter (1993), Sedimentary evolution of the Bounty Trough: A Cretaceous rift basin, southwestern Pacific Ocean, in *Sedimentary Basins of the World*, vol. 2, *South Pacific Sedimentary Basins*, edited by P. F. Ballance, pp. 51–67, Elsevier Sci., New York.
- Carter, R. M., L. Carter, and B. Davy (1994), Seismic stratigraphy of the Bounty Trough, south-west Pacific Ocean, *Mar. Petrol. Geol.*, **11**, 79–93.
- Christensen, N. I. (1996), Poisson's ratio and crustal seismology, *J. Geophys. Res.*, **101**, 3139–3156.
- Dauteuil, A., P. Huchon, F. Quemeneur, and T. Souriot (2001), Propagation of an oblique spreading centre: The western Gulf of Aden, *Tectonophysics*, **332**, 423–442.
- Davy, B. (1993), The Bounty Trough—Basement structure influences on sedimentary basin evolution, in *Sedimentary Basins of the World*, vol. 2, *South Pacific Sedimentary Basins*, edited by P. F. Ballance, pp. 69–92, Elsevier Sci., New York.
- Davy, B. (2006), Bollons Seamount and early New Zealand–Antarctic seafloor spreading, *Geochem. Geophys. Geosyst.*, **7**, Q06021, doi:10.1029/2005GC001191.
- Davy, B., and R. Wood (1994), Gravity and magnetic modelling of the Hikurangi Plateau, *Mar. Geol.*, **118**, 139–151.
- Davey, F. J. (1977), Marine seismic measurements in the New Zealand Region, *N. Z. J. Geol. Geophys.*, **20**, 719–777.
- Digranes, P., R. Mjelde, S. Kodaira, H. Shimamura, T. Kanazawa, H. Shiobara, and E. W. Berg (1996), Modelling shear waves in OBS data from the Vøring Basin (northern Norway) by 2-D ray-tracing, *Pure Appl. Geophys.*, **148**, 611–629.
- Digranes, P., R. Mjelde, S. Koaira, H. Shimamura, T. Kanazawa, H. Shiobara, and E. W. Berg (1998), A regional shear-wave velocity model in the central Vøring Basin, N. Norway, using three-component ocean bottom seismographs, *Tectonophysics*, **293**, 157–174.
- Dugda, M. T., A. A. Nyblade, J. Julia, C. A. Langston, C. J. Ammon, and S. Simiyu (2005), Crustal structure in Ethiopia and Kenya from receiver function analysis: Implications for rift development in eastern Africa, *J. Geophys. Res.*, **110**, B01303, doi:10.1029/2004JB003065.
- Eagles, G., K. Gohl, and R. D. Larter (2004), High-resolution animated tectonic reconstruction of the South Pacific and west Antarctic Margin, *Geochem. Geophys. Geosyst.*, **5**, Q07002, doi:10.1029/2003GC000657.

- Ebinger, C. J., and M. Casey (2001), Continental breakup in magmatic provinces: An Ethiopian example, *Geology*, *29*, 527–530.
- Fitzgerald, P. (2002), Tectonics and landscape evolution of the Antarctic plate since the breakup of Gondwana, with an emphasis on the west Antarctic rift system and the Transantarctic Mountains, *R. Soc. N. Z. Bull.*, *35*, 453–469.
- Forster, M. A., and G. S. Lister (2003), Cretaceous metamorphic core complexes in the Otago Schist, New Zealand, *Aust. J. Earth Sci.*, *50*, 181–198.
- Godfrey, N. J., F. J. Davey, T. Stern, and D. Okaya (2001), Crustal structure and thermal anomalies of the Dunedin Region, South Island, New Zealand, *J. Geophys. Res.*, *106*, 30,835–30,848.
- Gohl, K. (Ed.) (2003), Structure and dynamics of a submarine continent: Tectonic-magmatic evolution of the Campbell Plateau (New Zealand), report, Ber. zur Polarforsch., Alfred Wegener Inst. für Polar und Meeresforsch., Bremerhaven, Germany.
- Gray, G. G., and I. O. Norton (1988), A palinspastic Mesozoic plate reconstruction, *Tectonophysics*, *155*, 391–399.
- Herzer, R. (1995), Seismic stratigraphy of a buried volcanic arc, Northland, New Zealand and implications for Neogene subduction, *Mar. Petrol. Geol.*, *12*, 511–531.
- Ilichenko, T. (1996), Dniepr-Donets Rift: Deep structure and evolution from DSS profiling, *Tectonophysics*, *286*, 83–98.
- Kamp, P. J. J. (1986), Late Cretaceous-Cenozoic tectonic development of the southwest Pacific region, *Tectonophysics*, *121*, 225–251.
- Keranen, K., S. L. Klempere, R. Gloaguen, and EAGLE Working Group (2004), Three-dimensional seismic imaging of a protoridge axis in the main Ethiopian rift, *Geology*, *32*, 949–952.
- Kimbrough, D. L., A. J. Tulloch, D. S. Coombs, C. A. Landis, M. R. Johnston, and J. M. Mattinson (1994), Uranium-lead zircon ages from the Median Tectonic Zone, New Zealand, *N. Z. J. Geol. Geophys.*, *37*, 393–419.
- Krause, D. C. (1966), Geology and geomagnetism of the Bounty Trough, east of the South Island, New Zealand, *N. Z. Oceanogr. Inst. Mem.*, *30*, 34 pp.
- Laird, M. G. (1993), *Cretaceous Continental Rifts: New Zealand Region*, pp. 37–49, Elsevier Sci., New York.
- Latin, D., and N. White (1990), Generating melt during lithospheric extension: Pure shear vs. simple shear, *Geology*, *18*, 327–331.
- LeMasurier, W. E., and C. A. Landis (1996), Mantle-plume activity recorded by low-relief erosion surfaces in west Antarctica and New Zealand, *GSA Bull.*, *108*, 1450–1466.
- Lister, G. A., M. A. Etheridge, and P. A. Symonds (1986), Detachment faulting and the evolution of passive continental margins, *Geology*, *14*, 246–250.
- Louden, K. E., and D. Chian (1999), The deep structure of non-volcanic rifted continental margins, *Philos. Trans. R. Soc. London, Ser. A*, *357*, 767–805.
- Luyendyk, B. P., D. S. Wilson, and C. S. Siddoway (2003), Eastern margin of the Ross Sea Rift in western Marie Byrd Land, Antarctica: Crustal structure and tectonic development, *Geochem. Geophys. Geosyst.*, *4*(10), 1090, doi:10.1029/2002GC000462.
- Lytche, M. B., D. G. Vaughan and the BEDMAP Consortium (2000), *BEDMAP—Bed Topography of the Antarctic*, Br. Antarct. Surv., Cambridge, U. K.
- McAdoo, D. C., and S. Laxon (1997), Antarctic tectonics: Constraints from an ERS-1 satellite marine gravity field, *Science*, *276*, 556–560.
- Mortimer, N., F. J. Davey, A. Melhuish, J. Yu, and N. J. Godfrey (2002), Geological interpretation of a deep seismic reflection profile across the Eastern Province and Median Batholith, New Zealand: Crustal architecture of an extended Phanerozoic convergent orogen, *N. Z. J. Geol. Geophys.*, *45*, 349–363.
- Musacchio, G., W. D. Mooney, J. H. Luetgert, and N. I. Christensen (1997), Composition of the crust in the Grenville and Appalachian provinces of North America inferred from v_p/v_s ratios, *J. Geophys. Res.*, *102*, 15,225–15,241.
- Pedersen, T., and P. van der Beek (1994), Extension and magmatism in the Oslo Rift, southeast Norway: No sign of a mantle plume, *Earth Planet. Sci. Lett.*, *123*, 317–329.
- Ritzwoller, M. H., N. M. Shapiro, A. L. Levshin, and G. M. Leahy (2001), Crustal and upper mantle structure beneath Antarctica and surrounding oceans, *J. Geophys. Res.*, *106*(B12), 30,645–30,670.
- Ro, H. E., and J. I. Faleide (1992), A stretching model for the Oslo Rift, *Tectonophysics*, *208*, 19–36.
- Sandwell, D. T., and W. H. F. Smith (1997), Global seafloor topography from satellite altimetry and ship depth soundings, *Science*, *277*, 1956–1962.
- Scherwath, M., T. Stern, F. Davey, D. Okaya, W. S. Holbrook, R. Davies, and S. Kleffmann (2003), Lithospheric structure across oblique continental collision in New Zealand from wide-angle P wave modeling, *J. Geophys. Res.*, *108*(B12), 2566, doi:10.1029/2002JB002286.
- Smith, W. H. F., and D. T. Sandwell (1997), Marine gravity anomaly from Geosat and ERS 1 satellite altimetry, *J. Geophys. Res.*, *102*, 10,039–10,054.
- Spörli, K. B., and P. F. Ballance (1989), Mesozoic-Cenozoic ocean floor/continent interaction and terrane configuration, southwest Pacific area around New Zealand, in *The Evolution of the Pacific Ocean Margins*, edited by Z. Ben-Avraham, *Oxford Monogr. Geol. Geophys.*, *8*, 176–190.
- Sutherland, R. (1999), Basement geology and tectonic development of the greater New Zealand region: An interpretation from regional magnetic data, *Tectonophysics*, *308*, 341–362.
- Tamaki, K. (1985), Two modes of back-arc spreading, *Geology*, *13*, 475–478.
- Van Avendonk, H. J. A., W. S. Holbrook, D. Okaya, J. K. Austin, F. Davey, and T. Stern (2004), Continental crust under compression: A seismic refraction study of South Island Geophysical Transect I, South Island, New Zealand, *J. Geophys. Res.*, *109*, B06302, doi:10.1029/2003JB002790.
- Wandres, A. M., J. D. Bradshaw, S. D. Weaver, R. Maas, T. R. Ireland, and N. Eby (2004), Provenance analysis using conglomerate clast lithologies: A case study from the Pahau terrane of New Zealand, *Sediment. Geol.*, *167*, 57–89.
- Wernicke, B., and B. C. Burchfiel (1982), Modes of extensional tectonics, *J. Struct. Geol.*, *4*, 105–115.
- Wessel, P., and W. H. F. Smith (1998), New, improved version of generic mapping tools released, *Eos Trans. AGU*, *79*(47), 579.
- White, R. S., and D. H. Matthews (1980), Variations in oceanic upper crustal structure in a small area of the northeastern Atlantic, *Geophys. J. R. Astron. Soc.*, *61*, 401–431.
- Whitmarsh, R. B., G. Manatschal, and T. A. Minihull (2001), Evolution of magma-poor continental margins from rifting to seafloor spreading, *Nature*, *413*, 150–154.
- Winberry, J. P., and S. Anandkrishnan (2004), Crustal structure of the west Antarctic rift system and Marie Byrd Land hotspot, *Geology*, *32*, 977–980.
- Wood, R., and R. Herzer (1993), The Chatham Rise, New Zealand, in *Sedimentary Basins of the World*, vol. 2, *South Pacific Sedimentary Basins*, edited by P. F. Ballance, pp. 329–349, Elsevier Sci., New York.
- Woodcock, N. H. (2004), Life span and fate of basins, *Geology*, *32*, 685–688.
- Yegorova, T. P., R. A. Stephenson, V. G. Kozlenko, V. I. Starostenko, and O. V. Legostaeva (1999), 3-D gravity analysis of the Dniepr-Donets Basin and Donbas Foldbelt, Ukraine, *Tectonophysics*, *313*, 41–58.
- Zelt, C. A. (1999), Modelling strategies and model assessment for wide-angle seismic traveltimes data, *Geophys. J. Int.*, *139*, 183–204.
- Zelt, C. A., and D. A. Forsyth (1994), Modelling wide-angle seismic data for crustal structure: Grenville Province, *J. Geophys. Res.*, *99*, 11,687–11,704.
- Zelt, C. A., and R. B. Smith (1992), Seismic traveltimes inversion for 2-D crustal velocity structure, *Geophys. J. Int.*, *108*, 16–34.

D. Barker and B. Davy, GNS Science, 1 Fairway Drive, Avalon, Lower Hutt 5010, P.O. Box 30368, Lower Hutt 5040, New Zealand.

T. Deen, British Antarctic Survey, High Cross, Madingley Road, Cambridge, CB3 0ET, UK.

K. Gohl and G. Uenzelmann-Neben, Alfred Wegener Institute for Polar and Marine Research, P.O. Box 120161, 27515 Bremerhaven, Germany.

J. W. G. Grobys, Federal Armed Forces Underwater Acoustics and Marine Geophysics Research Institute, Klausdorfer Weg 2-24, 24148 Kiel, Germany. (jangurobys@bwb.org)